

PCCP

Accepted Manuscript



This is an *Accepted Manuscript*, which has been through the Royal Society of Chemistry peer review process and has been accepted for publication.

Accepted Manuscripts are published online shortly after acceptance, before technical editing, formatting and proof reading. Using this free service, authors can make their results available to the community, in citable form, before we publish the edited article. We will replace this *Accepted Manuscript* with the edited and formatted *Advance Article* as soon as it is available.

You can find more information about *Accepted Manuscripts* in the [Information for Authors](#).

Please note that technical editing may introduce minor changes to the text and/or graphics, which may alter content. The journal's standard [Terms & Conditions](#) and the [Ethical guidelines](#) still apply. In no event shall the Royal Society of Chemistry be held responsible for any errors or omissions in this *Accepted Manuscript* or any consequences arising from the use of any information it contains.

Halogen Bonding Interaction of Chloromethane with Several Nitrogen Donating Molecules: Addressing the Nature of the Chlorine Surface σ -hole

Pradeep R. Varadwaj,¹ Arpita Varadwaj, Bih-Yaw Jin¹

Department of Chemistry, National Taiwan University, Taipei, 10617, Taiwan

Abstract

With a view to understand the reason for the specific binding affinity of the chlorine in the $\text{H}_2\text{C}=\text{O}\cdots\text{Cl}-\text{CH}_3$ complex, we performed molecular electrostatic surface potential (MESP) analysis for isolated $\text{H}_3\text{C}-\text{Cl}$ with B3PW91, M06-2X, and MP2(full), all in conjunction with twenty-three Dunning- and Pople-type basis sets of double- and triple- ζ valence qualities. The results obtained are benchmarked against the best level of theory employed, CCSD/6-311++G(3d,2p). It is found that the local most maximum of ESP $V_{s,\text{max}}$ on the chlorine along the outermost extension of the C-Cl bond in $\text{Cl}-\text{CH}_3$ would vary dramatically from slightly negative to slightly positive values with respect to the basis set sizes and correlation methods employed. Its value mapped on the 0.001 electrons/bohr³ isodensity surface is ca. +1.0 kcal mol⁻¹ at the best level. This specific nature of the chlorine's $V_{s,\text{max}}$ is ipso facto more plausible, and is clarified considering the 0.0015- and 0.002-electrons/bohr³ isodensity envelopes, in which cases, $V_{s,\text{max}}$ is apparently small and positive despite the varied basis sets and methods utilized. The thirteen binary complexes investigated using MP2(full)/6-311++G(3d,2p) are thus resulted upon the interaction of chlorine's positive σ -hole in $\text{Cl}-\text{CH}_3$ with the local most negative areas of electrostatic potential $V_{s,\text{min}}$ confined on the nitrogen in the RN series of thirteen monomers, where RN = FCN, ClCN, BrCN, CH_3CN , HOCN, HSCN, PCCN, PN, CCl_3CN , SiH_3CN , NCCN, CNCN, and NaCN. In all the instances, the $\text{N}\cdots\text{Cl}$ intermolecular distances of separation evaluated are less than the sum of the chlorine and nitrogen van der Waals radii, 3.48 Å. The $\text{N}\cdots\text{Cl}$ contacts are all stable, and are having quasi-linear geometries ($\angle\text{N}\cdots\text{Cl}-\text{C} \cong 175\text{--}180^\circ$), unraveling the directional nature of the chlorine's positive σ -hole. The effect of substituents -R on binding energies ΔE of the $\text{RN}\cdots\text{Cl}-\text{CH}_3$ complexes is found to be marginal, values ranging from -0.39 and -1.29 kcal mol⁻¹ with MP2(full) and that from -0.02 to -0.84 kcal mol⁻¹ with CCSD(T). Applications of atoms in molecules and noncovalent interaction reduced-density-gradient methods revealed the $\text{N}\cdots\text{Cl}$ interactions to be of electrostatic origin. The red- and blue-shifts in the vibrational stretching frequencies of the C-Cl bonds estimated with the MP2(full) are found to be accompanied with the increase and decrease in the corresponding bonds upon formation of the $\text{RN}\cdots\text{Cl}-\text{CH}_3$ complexes, respectively. Natural bond orbital analysis showed that there are several weak interorbital charge transfer interactions persisting between the electron-acceptor and -donor orbitals of the monomers interacting in the $\text{RN}\cdots\text{Cl}-\text{CH}_3$ complexes.

¹ Corresponding Author's Email Addresses: pradeep@t.okayama-uc.jp (PRV), byjin@ntu.edu.tw (BYJ)

Tel: +886-2-33661165, Fax: +886-2-23636359

1. Introduction

One of the most appealing developments in chemistry with increased recent interest in non-covalent interactions is halogen and other σ -hole bonding interactions.¹ Initial interests in most of these studies lie with, among other things, four principal issues. One of it was to understand why the negatively charged halogen in one molecule could make long-range contacts with the negatively charged sites in other molecules in many crystallographically stabilized structures.² A second interest was to explore factors that best elucidate the chemical physics and anisotropic nature of halogens.^{2d-2f} A third interest was to develop a firm understanding on whether these and other factors are responsible in determining the geometrical stabilities of the $D\cdots X-A$ interactions.^{2e-2g} In $D\cdots X-A$, D is an electron donor and A is an electron deactivating (ED) atom or a fragment covalently bonded to halogen X; the commonly studied ED groups include, among others, $-\text{NO}_2$, $-\text{C}\equiv\text{N}$, $-\text{CX}_3$ (X = F, Cl, Br, I) and $-\text{X}$ (X = F, Cl, Br, I).¹⁻² And, the fourth one was to identify and develop novel experimental and theoretical strategies that could best describe the three former issues. It is worth noting that halogen and other σ -hole bonding interactions are competitive with $D\cdots H-A$ hydrogen bonds,^{1a,1b,1f, 1g,1k} and are more sensitive to tunability, have strong directional preferences for bonding, and are widely responsible in explaining many phenomenological processes in chemistry and molecular biology,^{1g,1h,} and in the design of drugs^{1l} and engineered supramolecular materials.^{1g,1h,1k}

We are in particular interested in σ -hole interactions. σ -holes are a special kind of electropositive electron-deficient regions along the outermost extensions of covalent bonds to halogens in molecules, this concept was first introduced in 2007.^{1e} Many recent studies reveal that σ -holes can also show up on particular main group atomic surfaces (e.g., elements of groups 14 – 16) when they are covalently bonded to A.^{3, 4} This is because the deactivating group pulls electron densities towards the covalent bond through its interaction with the main group atoms in molecules, leaving behind a small region of depleted electron density on the outer lobe of the covalent bonds.^{1a,1c,3,4} The σ -hole therefore acts like a tiny activated magnetic attractor which is skilled enough to pull electron rich negative centers, such as Lewis base centers, on another molecules towards itself to form electrostatically stabilized long-range contacts, thereby giving particular shapes to the resulting complex geometries.¹⁻⁴

The molecular electrostatic surface potential model best describes the σ -holes. It determines the local most maxima and minima values of electrostatic potential ($V_{s,\text{min}}$ and $V_{s,\text{max}}$, respectively) on atomic surfaces in molecules.^{1c,1e} In general, these appear around the lateral- and along the axial-sites of an atom X on the extension of the A-X covalent bond, respectively, which can be either positive or negative depending on the nature of the substituents A in A-X. For example, in hydrogen halides H-X the halogen (σ -hole) $V_{s,\text{max}}$ are ca. -19.38 , $+9.34$, and $+15.95$ kcal mol⁻¹ on the outermost extensions of the H-F, H-Cl, and H-Br covalent bonds, respectively, obtained using MP2(full)/6-311++G(3d,2p). These results show that with increasing the electronegativity of the halogens the strength of the σ -holes gradually increases from X = F to Cl to Br. This trend in $V_{s,\text{max}}$ is more general, observed for many different series,^{1g,3a,4d} including, for example, the methyl halides X-CH₃ (X = F, Cl, Br), where F-CH₃ (C-F = -21.0) <

Cl-CH₃ (C-Cl = -1.5) < Br-CH₃ (C-Br: +5.9) with B3PW91/6-31G(d,p), values in kcal mol⁻¹ mapped on their corresponding 0.001 au (electrons/bohr³) isodensity surfaces.¹⁹

A positive σ -hole ($V_{s,max} > 0$) in a molecule is always prone to engage in establishing noncovalent interactions with negative sites ($V_{s,min} < 0$) occupied on another molecules, leading to the formation of σ -hole bonding interactions.^{1e,1g,2,3,4} This widespread view adequately explains vast majorities of donor-acceptor interactions comprising of atoms of groups from 14 to 17, thus is more general no matter what computational methodology is used,⁴⁻⁵ but the detail of the nature of these interactions is still a topic of many discussions because of their complexities.^{5h} For some of the group 14-16 atoms, which are more electronegative, the $V_{s,max}$ are negative ($V_{s,max} < 0$) along the outer extensions of the covalent bonds (e.g., H-F), and consequently they are not expected to engage in σ -hole bonding interactions with other molecules according to Politzer et al.^{4d}

Several authors pointed out that σ -hole theory does not explain an existing noncovalent interaction in certain heterodimers.^{1c,1e,1g,1l,2a,5} One such example is the H₂C=O...Cl-CH₃ complex. According to Clark et al^{1e} and Politzer et al^{1c} the combined effects of the chlorine's high electronegativity and the significant sp-hybridization along the C-Cl bond cause an influx of electronic charge that neutralizes the σ -hole on the outermost portion of the chlorine, it therefore cannot σ -hole bond with the negative site on other molecules, an interpretation which may be in agreement with that of others.⁶ This argument seemingly fact-based for F-CH₃ is also applicable to the fluorine in CF₄ because, according to refs,^{1c,1e,4d} the halogen surfaces in these molecules are entirely negative. To our view, this interpretation may be true for the fluorine in F-CH₃ given its electronegativity χ is markedly large compared to the other three members of the halogen family ($\chi(\text{F}) = 3.98$ vs. $\chi(\text{Cl}) = 3.16$, $\chi(\text{Br}) = 2.96$, and $\chi(\text{I}) = 2.66$).^{7a} However, it should not be the case for the chlorine in Cl-CH₃ given the electronegativity and polarizability of atomic chlorine are perceptibly large compared to that of the fluorine (atomic polarizabilities for respective atoms are ca. 2.18 and 0.557, in units of 10⁻²⁴ cm³).^{7b} Nevertheless, the specific suggestions made in refs.^{1c,1e,1g,2,4d} do not match with the justifications of Riley and Hobza,^{5b} who have showed that the outermost portion of the chlorine in Cl-CH₃ along the C-Cl bond is capable of establishing a long-range contact with the negative oxygen center in formaldehyde (H₂C=O), leading to the formation of the H₂C=O...Cl-CH₃ complex. Palusiak demonstrated that formation of this complex is unstable with BP86/QZ4P,^{6c} whilst Riley et al suggested that the stability of this complex is predominantly determined by the electrostatic and dispersion interaction components that contribute significantly to its binding energy.^{5b} Supporting this latter view of Riley et al,^{5b} Politzer et al¹⁹ added in saying that the polarizing effect of the oxygen in H₂C=O is evidently enough to induce a positive potential on the chlorine, which is then responsible for the formation of the H₂C=O...Cl-CH₃ complex, which we believe to be misleading.

Moreover, in 2012, Eskandari and Zariny provided a compact lump-hole topological model^{5c} description to validate the genuineness of the σ -hole bonding interaction in the H₂C=O...Cl-CH₃ complex. However, according to them, the σ -hole concept is effective only when electrostatic forces play a predominant role to stabilize the halogen-bonded complexes, and that it fails when other energy

components, such as dispersion, contribute significantly to the binding energies, a view which is seemingly perversely counterintuitive. By contrast, in 2013, Clark^{5e} asserts that *despite the chlorine in CH₃-Cl is not having a positive σ -hole, however, the H₂C=O \cdots Cl-CH₃ complex formation appears to be due to polarization by the halogen-bond acceptor, in conjunction with dispersion.* Incontrovertibly, from the varied interpretations made by several authors, there is no way of saying whose conclusion captures reality on the nature of the σ -hole in Cl-CH₃. Towards this end, one of the main goals of this paper to reexamine why the σ -hole concept cannot explain the noncovalent bonding observed in H₂CO \cdots Cl-CH₃. To be precise, we examine whether this above failure is a conceptual shortcoming of the σ -hole theory or simply an artefact of the levels of theory previously employed?

Interest in the chemistry of Cl-CH₃ stems from its importance, among other things, as a hazardous substance (leading to the risk of chronic health effect, cancer and death),^{8a,8b} as a chlorine-containing supplier to the stratosphere,^{8c} as an intermediate in the production of silicone polymers,^{8d} as a solvent in industry,^{8b} as a paint stripper for coating remover,^{8b,8e} as a herbicide,^{8f} and as chlorinating and methylating agents in environmental organic reaction chemistry.^{8g,8h} Studies on the hydrogen bond accepting ability of the chlorine in Cl-CH₃ are also carried out in the past,^{9a-9b} which shows that the lateral sides of the chlorine can make a long-range contact with the H atom of its binding partner H-Cl, in agreement with experiment.^{9c} This may be reasonable given the lateral sides of the chlorine in Cl-CH₃ are very negative ($V_{s,\min} = -14.45 \text{ kcal mol}^{-1}$, Figure 1). However, as noted above, the chlorine in Cl-CH₃ has a negative $V_{s,\max}$ on its surface is already ossified into a dogma, thus its nature needs to be clarified to demonstrate its σ -hole-donating capacity.

In this paper, we aim at investigating how, and to what extent, the sign and magnitude of the chlorine σ -hole $V_{s,\max}$ in Cl-CH₃ would vary on its 0.001 au isodensity surface with respect to the two most promising and most frequently used Density Functional Theory (DFT) functionals (B3PW91^{10a} and M06-2X^{10b}), in conjunction with twenty-three basis sets of Pople and Dunning types. We benchmark these results against the best levels of theory employed, the second-order Møller-Plesset MP2(full)^{10c} and Coupled Cluster Singles and Doubles CCSD methods,^{10d} where full means all electrons of Cl-CH₃ are included in the correlation treatment. Secondly, we compute the chlorine $V_{s,\max}$ on the 0.0015-, and 0.002-au isodensity surfaces with some of these methods/basis sets to see how these results compare and contrast with the results already obtained on the corresponding 0.001 au isodensity surface of the molecule. Thirdly, we consider several molecules containing nitrogen donors to demonstrate whether the chlorine σ -hole in Cl-CH₃ can indeed essentially form linear σ -hole bonds with the negative nitrogen sites of the R-N series of thirteen molecules, and whether one can expect general signatures as one might expect for halogen- and other σ -hole bonding interactions, where R = FC, ClC, BrC, CH₃C, HOC, HSC, PCC, P, CCl₃C, SiH₃C, NCC, CNC, and NaC. Towards this end, our main interest is to investigate the extent to which the -R portions of the nitrogen donor molecules influences the structural, electronic, and binding energy properties of the modified complexes. We apply Quantum Theory of Atoms in Molecules

(QTAIM),¹¹ NonCovalent Interaction Reduced Density Gradient (NCI-RDG),¹² and Natural Bond Orbital (NBO)¹³ techniques to achieve insight significantly into the intermolecular interactions in the $\text{RN}\cdots\text{Cl}-\text{CH}_3$ complexes. Finally, we attempt to cross-correlate various (intermolecular) topological and non-topological bonding properties revealed by these theoretical methods to provide insight into whether at least which of these properties can be best used to serve as indicators of complex stability.

2. Computational methodologies

The B3PW91^{10a} and M06-2X^{10b} DFT functionals implemented in Gaussian 09¹⁴ are recommended for the calculation of the molecular electrostatic surface potential (MESP).^{1c, 1g, 3a, 4d, 5h} Thus for isolated $\text{Cl}-\text{CH}_3$, these two DFT functionals, together with the MP2(full) and CCSD,^{10c} all in conjunction with twenty-three double- and triple- ζ basis sets of Dunning- and Pople-types, are employed to optimize its C_{3v} geometry. The six Dunning's type basis sets include cc-pVDZ, cc-pVTZ, aug-cc-pVDZ, aug-cc-pVTZ, jul-cc-pV(D+d)Z, and jul-cc-pV(T+d)Z. The seventeen Pople's type basis sets include 6-31G(d), 6-31G(d,p), 6-31G(2d,p), 6-31G(2d,2p), 6-31+G(d,p), 6-31++G(d,p), 6-31++G(2d,p), 6-31++G(2d,2p), 6-311G(d), 6-311G(d,p), 6-311G(2d,p), 6-311(2d,2p), 6-311+G(d,p), 6-311+(2d,2p), 6-311++G(d,p), 6-311++G(2d,2p), and 6-311++G(3d,2p). Tight SCF convergence and ultrafine integration grid criteria instead of default settings are impetrated for DFT calculations.

To explore the reactive behavior of the various atomic and inter-atomic regions present in the fourteen isolated molecules, analyses of the MESP^{1g,2,3,5} are carried out using MultiWfn code.¹⁵ Eq. 1 implemented in this code relates the molecular electrostatic potential $V(r)$ of a given molecule due to its nuclei and electrons at any point r to its molecular electron density $\rho(r)$, where Z_A is the charge on nucleus A located at position R_A .

$$V(r) = V_{nuclei} + V_{electrons} = \sum_A \frac{Z_A}{|r - R_A|} - \int \frac{\rho(r')dr'}{|r - r'|} \dots\dots\dots(1)$$

The energy-minimized geometries obtained for $\text{Cl}-\text{CH}_3$ are used for generating the wavefunction files, which were then supplied to MultiWfn code¹⁵ for evaluating the $V_{s,\text{max}}$ and $V_{s,\text{min}}$ on the corresponding 0.001 au isodensity surfaces of the $\text{Cl}-\text{CH}_3$ molecule. For reasons discussed later, the MESP calculations for the $\text{Cl}-\text{CH}_3$ molecule are also performed on the 0.0015- and 0.002-au isodensity surfaces. And, for the other thirteen monomers, the MESP are examined on their respective 0.001-, 0.0015-, and 0.002-au isodensity surfaces only with MP2(full)/6-311++G(3d,2p). All these above results are benchmarked against the CCSD/6-311++G(3d,2p).

The geometries of all the thirteen binary complexes formed between CH_3-Cl and the other thirteen monomers are optimized using MP2(full) and CCSD, both in conjunction with 6-311++G(3d,2p).

The keyword Density=Current was requested during these calculations. Because the Hessian second derivative calculations are very extensive even for small complexes with CCSD/6-311++G(3d,2p), we have performed these calculations only at the MP2(full)/6-311++G(3d,2p) level on the corresponding energy-minimized geometries of the monomers and complexes to exploit the vibrational characteristics. The resulting positive Hessian eigenvalues confirmed the true nature of the energy-minimized geometries of both the monomers and complexes.¹⁶ For graphical analyses of the normal mode vibrational frequencies and presentation of the molecular electrostatic surface potential maps the Gaussview 05¹⁷ and AIMALL¹⁸ packages are used, respectively.

To comprehend whether the Cl-CH₃ subunit forms stable complexes with the RN series of thirteen molecules, eqs. 2 is used for calculating the binding energy, ΔE , between the two monomers in each of the RN...Cl-CH₃ complexes without incorporating the effect of the zero-point vibrational motion. In this eqn., the terms E_T on the right-hand-side are the uncorrected total electronic energies at 0 K that refer to both the isolated and complexed species.

$$\Delta E = E_T(\text{RN}\cdots\text{Cl-CH}_3)_{\text{complex}} - (E_T(\text{RN}) + E_T(\text{Cl-CH}_3)) \dots \dots \dots (2)$$

QTAIM¹¹ calculations are performed using AIMALL¹⁸ to obtain various topological parameters and to insight into various closed-shell (electrostatic) and opened-shell (shared) interactions involved in the RN...Cl-CH₃ complexes.

Further calculations are performed with the RHF/6-31+G(d,p) method on the MP2(full)/6-311++G(3d,2p) optimized geometries of the RN...Cl-CH₃ complexes to evaluate the second order perturbative estimates of electron charge transfer delocalization energies, $E^{(2)}$, operating between the donor (i) and acceptor (j) NBOs. Eq. 3 represents to the expression that governs $E^{(2)}$, where ε_i and ε_j are the diagonal orbital energies of the donor (i) and acceptor (j) NBOs, respectively, q_i is the donor orbital occupancy, and $F_{(i,j)}$ is the off-diagonal NBO Fock matrix element. NBO programs¹³ incorporated in Gaussian 09¹⁴ was employed for this purpose.

$$E^{(2)} = \Delta E_{ij} = q_i \frac{F_{(i,j)}^2}{\varepsilon_i - \varepsilon_j} \dots \dots \dots (3)$$

To discern how effective are the nature of charge rearrangements and the changes in the molecular polarities that accompany complex formation, the integrated charges (q) and dipole moments (μ) are calculated using Eqs. 4 and 5, respectively.¹⁹ In Eq. 4, $q(\Omega)$ is the electronic charge associated with atom Ω , Z_Ω is the charge of the nucleus of atom Ω , $\rho(r)$ is the molecular charge density, and the integration extends over the entire basin of atom Ω . In Eq. 5, r_Ω is the position vector with the origin is

located at the nucleus of atom Ω , R_Ω is the position of the nucleus of atom Ω in the arbitrary molecular coordinate system, $\rho(r)$ is the molecular electron density function, and the sum and integration run over all atoms in the molecule or that in the molecular complex. Without any specific bias, the MP2(full)/6-311++G(3d,2p) optimized geometries are used to obtain the charge and dipole moments of the monomers and complexes at the same level.

$$q(\Omega) = Z_\Omega - \int_\Omega \rho(r) dr \dots\dots\dots(4)$$

$$\mu = \sum_\Omega \mu_\Omega = \sum_\Omega [-\int_\Omega r_\Omega \rho(r) dr + q(\Omega)R_\Omega], \quad r = r_\Omega + R_\Omega \dots\dots\dots(5)$$

NonCovalent Interaction (NCI) Reduced Density Gradient (RDG) method is recently proposed for studying noncovalent interactions.¹² The theory relies on two scalar properties, charge density ρ and reduced-density-gradient (RDG, s), which are related to each other by Eq. 6. We apply this method to unravel the nature of the intermolecular bonding interactions in the $RN \cdots Cl-CH_3$ complexes.

$$s = \frac{1}{2(3\pi^2)^{1/3}} \frac{|\nabla\rho|}{\rho^{4/3}} \dots\dots\dots(6)$$

The extent of electron pairs delocalized in each pair of two atomic basins $\delta(\Omega_A, \Omega_B)$ in the $RN \cdots Cl-CH_3$ complexes is determined using Eq. 7.²⁰ In this Eq., the indices a and b in summations run over all the $N/2$ occupied molecular orbitals, and $S_{ab}(A)$ and $S_{ab}(B)$ are the molecular orbital overlap integrals over respective atomic basins Ω_A and Ω_B .

$$\delta(\Omega_A, \Omega_B) = 4 \sum_a \sum_b S_{ab}(A) S_{ab}(B) \dots\dots\dots(7)$$

3. Results and discussions

3.1 Monomer properties

Table 1 summarizes the MP2(full)/6-311++G(3d,2p) and CCSD/6-311++G(3d,2p) calculated monomer electric dipole moments μ , the zero-point vibrational energies ZPVE, the C-Cl, P-N and C-N bond distances r , and the nitrogen $V_{s,\min}$ along the outer extensions of the C-N and P-N bonds. The experimental data are also included wherever feasible. One may see from the table that there is a reasonable agreement between the MP2(full) and CCSD dipole moments for all the monomers, except for PCCN for which the latter method largely overestimates μ compared to the former. The C-Cl, P-N and C-

N bond distances are largely overestimated with the former method compared to the latter method. Other than this, the agreement between calculated and experimental μ and ZPVE values is reasonable, implying that the choice of the computational methodologies may be adequate to describe the physical properties of the $\text{RN}\cdots\text{Cl}-\text{CH}_3$ binary complexes investigated.

3.2 Nature of the electrostatic surface potential of the chlorine in CH_3Cl

Figure 1 illustrates the 0.001 au mapped MESP of the $\text{Cl}-\text{CH}_3$ molecule, obtained with MP2(full)/6-311++G(3d,2p). There are five small regions of positive electrostatic potential on its surface. One of it is on the carbon surface along the outer extension of $\text{Cl}-\text{C}$ bond, the second is on the chlorine surface localized along the outer extension of the $\text{C}-\text{Cl}$ bond, and the other three are on the three hydrogen surfaces, each along the outermost extension of the $\text{C}-\text{H}$ bond. The local most negative areas of electrostatic potential, which are degenerate, are located on the side-on portions of the chlorine surface. Of interest is the chlorine σ -hole which is found to have the smallest area of positive electrostatic potential, with $V_{s,\text{max}} = +1.52 \text{ kcal mol}^{-1}$. This result is in sharp disagreement Brinck et al,^{2a} Politzer et al,^{1c,1g,4d,5a} Murray et al,^{4b,4c,5h} Clark et al,^{1e,5g} and Ibrahim,^{5f} who have repeatedly suggested negative a $V_{s,\text{max}}$ on the chlorine surface in $\text{Cl}-\text{CH}_3$ (e.g., $V_{s,\text{max}}$ values were ca. -1.5 , -0.9 , -0.73 , and $-1.38 \text{ kcal mol}^{-1}$ with B3PW91/6-31G(d,p),^{1c} M06-2X/6-311G(d),^{5h} B3PW91/aug-cc-pVDZ,^{5f} and B3PW91/6-31G(d,p),^{5f} respectively).

Is this above 0.001 au isodensity surface mapped positive electrostatic potential of the chlorine sensitive to the level of correlated method (and basis sets) by which they are estimated? The answer is yes. Now, let us look at Table 2 which provides the complete details of the benchmark that contains 69 values of the chlorine $V_{s,\text{max}}$ for comparison, computed on the 0.001 au isodensity surfaces using three correlated methods and a variety of 23 basis sets. A number of conclusions of general interest can be drawn from these data. Undeniably, firstly, computations show a remarkable variation in the magnitudes as well as in the signs of the chlorine $V_{s,\text{max}}$, some predicts slightly negative values while some slightly positive, with the $V_{s,\text{max}}$ ranging from -2.16 to $+1.60 \text{ kcal mol}^{-1}$. The basis sets cc-pVDZ, aug-cc-pVDZ, and cc-pVTZ predict slightly negative $V_{s,\text{max}}$, whereas that of jul-cc-pV(D+d)Z and jul-cc-pV(T+d)Z predict slightly positive $V_{s,\text{max}}$ for the chlorine σ -hole with MP2(full), B3PW91 and M06-2X. On the other hand, the MP2(full) method gave negative $V_{s,\text{max}}$ for most of the double- ζ basis sets that do not include ++ and 2d polarization functions, and positive $V_{s,\text{max}}$ for most of the triple- ζ basis sets passing from 6-311G(d,p) to 6-311++G(d,2p). There is a few exception to this latter characteristic, in which, the $V_{s,\text{max}}$ is ca. -0.31 , -0.05 , and $+0.22 \text{ kcal mol}^{-1}$ with 6-311G(d), 6-31G(2d,p), and 6-311G(2d,2p), respectively. Contrastingly, the B3PW91 and M06-2X methods show some major deviations both in signs and magnitudes of the $V_{s,\text{max}}$, details given in Table 2. Secondly, we observe no specific trend in the $V_{s,\text{max}}$ obtained with the three correlated methods in conjunction with a given basis set, compared to those

obtained with these methods in conjunction with most of the other basis sets (this can be inferred comparing the $V_{s,max}$ values listed in the first four rows of Table 2, for example). However, the $V_{s,max}$ obtained with triple- ζ basis sets containing at least two sets of each of the d- and p-polarization functions eliminate the above discrepancy, in which cases, the $V_{s,max}$ follow a specific pattern: M06-2X < B3PW91 < MP2(full), which can be inferred comparing the $V_{s,max}$ values listed in the last four rows, for example. Clearly, the above results allow one to conclude that the MP2(full) outperforms the two DFT functionals, and that this method does not require additional diffuse and polarization functions to favorably predict a positive σ -hole ($V_{s,max} > 0$) on the chlorine's 0.001 au isodensity surface in H_3C-Cl . The result is in excellent agreement with the value of +1.01 kcal mol⁻¹, calculated with CCSD/6-311++G(3d,2p). From the aforementioned results, it is probably that the varied signs of the chlorine σ -hole $V_{s,max}$ are a consequence of the level of electron correlation, but in addition to this, the size of the basis set is one of the major factors that determines the sign of the chlorine $V_{s,max}$ in H_3C-Cl .

According to a reviewer, the signs and magnitudes of the chlorine $V_{s,max}$ obtained with various methods/basis sets are controversial, and there is no guarantee which method captures the reality. In this context, we prioritize that the evaluation of the MESP often relies on the 0.001 au isodensity surface, a surface that lies at a distance somewhat greater than the van der Waals radius of an atom in molecules.^{1c,1e,1g,2,29} A specific reason for selecting this particular surface, according to Politzer et al (that follows from a prior recommendation of Bader et al^{11a,30}), is that it reflects the properties of that molecule, viz., the lone pairs, electron occupancies, atomic volumes, strained bonds, etc.²⁹ These physical properties of the molecule, according to Bader and coworkers,³⁰ are also independent of the choice of the 0.001- and 0.002-au isodensity surfaces, as are large enough to contain at least 96% of the molecule's electronic charge, and lie within the usual limits of van der Waals contact distances. Accordingly, we extended our calculations to compute the chlorine $V_{s,max}$ on the 0.0015- and 0.002-au isodensity surfaces with MP2(full), and the results are collected in Table 2, and are compared with the corresponding 0.0015 au mapped results obtained with B3PW91 and M06-2X. Not surprisingly, the chlorine $V_{s,max}$ are found to be all small and positive on the 0.0015- and 0.002-au isosurfaces, again this is regardless of the nature of the twenty-three basis sets and the levels of electron correlation. The $V_{s,max}$ are ranging from +0.52 to +4.38 kcal mol⁻¹ and that from +2.45 to +6.84 kcal mol⁻¹ for the former and latter isosurfaces, respectively, but are indeed comparatively larger than those of the 0.001 au isodensity surface $V_{s,max}$. There is an exception for M06-2X/cc-pVDZ, in which case, a negative $V_{s,max}$ of -0.14 kcal mol⁻¹ is predicted on the 0.0015 au isodensity envelope, although this is again positive on the 0.002 au isodensity surface. Our above 0.0015- and 0.002-au mapped $V_{s,max}$ results are in agreement with a conclusion of Ibrahim,^{5f} and are confirmed by the CCSD calculations obtained in conjunction with aug-cc-pV(d+D)Z, aug-cc-pVTZ, aug-cc-pV(d+T)Z, and cc-pVQZ basis sets. For instance, the 0.0015 (0.002) au-

mapped $V_{s,max}$ values on the chlorine surface are ca. +1.15 (+3.48), +0.51 (+2.73), +1.88 (+4.21), and +1.50 (+3.70) kcal mol⁻¹ with these four levels of calculation, respectively. Our above conclusion is thus decisive, confirming the fact that chlorine's σ -hole is indeed having a positive electrostatic potential on its surface along the outermost extension of the C–Cl bond in H₃C–Cl. It is worth mentioning that this argument for H₃C–Cl is also applicable to the fluorines in tetrafluoromethane (CF₄), although their surfaces along the outermost extensions of the C–F bonds were demonstrated in several occasions to be entirely negative;^{1c,1g,2a,3a} we report our result elsewhere.

3.3 Binary complexes

3.3.1 Structural properties

Figure 2 illustrates the RN···Cl–CH₃ binary complexes examined. In each of the complexes in it, the chlorine in Cl–CH₃ is directed almost in the same line towards the oppositely placed nitrogen center in RN. An important geometrical parameter that gives some tentative information about the nature of bonding interaction between the monomers in the equilibrium structures of the complexes is the N···Cl internuclear distance of separation. As one sees from Table 3, this distance of separation is ranging from 3.1520 (for NaCN···Cl–CH₃) to 3.2055 Å (for SiH₃CN···Cl–CH₃) with MP2(full). The CCSD method, by contrast, predicts significantly larger N···Cl bond distances ranging from 3.3181 (for NaCN···Cl–CH₃) to 3.38277 (SiH₃CN···Cl–CH₃) Å. The contact distances predicted with both these methods are clearly < 3.48 Å, the sum of the van der Waals radii of the bonded nitrogen and chlorine atoms, r_{N+Cl} , in agreement with a IUPAC criterion,^{2g} where the van der Waals radii of nitrogen and chlorine are ca. 1.82 Å and 1.66 Å, respectively.³¹

Another very important structural information can be gleaned by inspecting the intermolecular bond angles existing between the first three or the last three atoms of the R–N···Cl–C motifs of the R–N···Cl–CH₃ complexes. These three atoms involved in the two geometrical arrangements are nearly linear in the first eleven complexes listed in Table 3, with $\angle R-N\cdots Cl \cong \angle N\cdots Cl-C \cong 179 - 180.0^\circ$, revealing the directional nature of the N···Cl σ -hole interactions.^{1g,4d} For HOCN···Cl–CH₃ (and HSCN···Cl–CH₃), however, the two angles associated with the R–N···Cl–C motif are $\angle C-N\cdots Cl \cong 175.3$ (and 175.2°) and $\angle N\cdots Cl-C \cong 179.8$ (and 179.6°), respectively, showing these angles to deviate largely from linearity. The CCSD method gave slightly different values for these two latter angles for the complexes, 174.8 (and 175.3°) vs. 179.8 (and 179.6°). The aforementioned nonlinearity is mainly due to the two monomers HSCN and HOCN which are having nonlinear $\angle SCN$ and $\angle OCN$ (i.e., $\angle SCN = 176.1$ (176.4°) with MP2 (CCSD) in isolated HSCN and $\angle OCN = 176.4$ (176.9°) with MP2(CCSD) in isolated HOCN). These results are probably in line with the third criterion of IUPAC,^{2g} according to which, in the D···X–A halogen-bond

the angle $D\cdots X-A$ tends to be close to 180° , i.e., the halogen bond acceptor D approaches X along the extension of the A-X bond.

3.3.2 Binding energy and its relationship with $V_{s,\min}$

The binding energy, ΔE , is an important measure of the strength of an intermolecular interaction. It gives some knowledge about the exothermic (as well as endothermic) nature of a reaction between the monomers. ΔE for the $RN\cdots Cl-CH_3$ complexes are calculated using Eq. 2, and the results are summarized in Table 3. Examination of the ΔE values reveals that they are all lying within a narrow range between -0.39 and -1.29 kcal mol $^{-1}$ with MP2(full), and that between -0.02 and -0.84 kcal mol $^{-1}$ with CCSD(T); the latter results show a substantial reduction of the ΔE values compared to the former method, a result which is in agreement with Bauzá et al for halogen bonded interactions,^{10e} and the negative sign indicates complex formation at 0 K. The change in the zero-point vibration energy, $\Delta ZPVE$, estimated with the former method, that accompanies complex formation is seemingly very small (see Table 3), thereby stressing its non-negligible effect on the magnitudes of ΔE . For instance, an inclusion of the $\Delta ZPVE$ will reduce the ΔE by between 0.20 and 0.28 kcal mol $^{-1}$ with MP2(full).

For comparison, Riley and Hobza^{5b} reported a CBS extrapolated ΔE value of -1.13 kcal mol $^{-1}$ for the $H_2CO\cdots Cl-CH_3$ complex using Symmetry Adapted Perturbation Theory, and interpreted this arising predominantly from electrostatic and dispersion interactions (-0.96 vs. -1.96 kcal mol $^{-1}$) after being compensated with contributions arising from induction and exchange repulsion (-0.23 vs. $+2.02$ kcal mol $^{-1}$). Whereas this result is in sharp disagreement with the observations of Palusiak who described the formation of the $H_2CO\cdots Cl-CH_3$ complex to be unstable with the Kohn-Sham molecular orbital model,^{6c} they found the interaction energies for the other two members of the series, $H_2CO\cdots X-CH_3$ ($X = Br$ and I), to be primarily due to charge transfer and polarization effects. Evidently, the results of the two energy-partitioning approaches adopted in the two above studies are contradictory to each other, showing that these methods are not physically rigorous. There is therefore no guarantee which part of the interaction energy (electrostatic, or polarization, or dispersion) will be the primary source for the stabilization of the above complexes.

As emphasized previously by us,^{3d,3f} as well as by others,³² the Basis Set Superposition Error (BSSE) correction for energy using the counterpoise procedure of Boys and Bernardi⁶⁰ needs to be accounted for with caution. This is likely for *ab initio* wave function theory correlated calculations because at these levels the BSSE jeopardizes the true physical quality of ΔE by predicting a large spurious and unphysical attractive energy between the monomers.^{32a,32b} To support this statement, we computed the BSSE only with the MP2(full) method, and the data summarized in Table 3 show that the values of the BSSE are to lie between 69% ($NCCN\cdots Cl-CH_3$) and 219.8% ($HO CN\cdots Cl-CH_3$) of ΔE .

The nitrogen in NCCN in the monomer series is found to have the least $V_{s,\min}$ (cf. Table 1), which is not surprising because there is a strong compromise between the two identical electron withdrawing –CN groups to pull electron densities from the two end sites of the molecule to the central bonding region. For the $\text{Na}^+\text{–CN}^-$ molecule, on the other hand, the Na^+ cation is having the weakest electron-withdrawing ability, which may explain why the nitrogen in this molecule is highly nucleophilic, occupying the largest negative area of electrostatic potential in the series (viz., $V_{s,\min}$ is -63.33 and -67.40 kcal mol $^{-1}$ with MP2(full) and CCSD(T), respectively). Even so, the nitrogen lone-pair in this species does not create a sufficiently strong electric field to bind strongly with the chlorine of $\text{CH}_3\text{–Cl}$. Thus the prior suggestion¹⁹ that the polarizing field of the oxygen lone pair in $\text{H}_2\text{C=O}$ will create a positive electrostatic potential on the surface of the chlorine in Cl–CH_3 , this will then bring the two monomers together to form the $\text{H}_2\text{O=C}\cdots\text{Cl–CH}_3$ complex, is deemed misleading.

From the data in Table 1, one may see that the 0.001 au mapped nitrogen $V_{s,\min}$ obtained with CCSD increases in this order: $\text{NC–C}\equiv\text{N} < \text{CN–C}\equiv\text{N} < \text{CCl}_3\text{–C}\equiv\text{N} < \text{F–C}\equiv\text{N} < \text{Cl–C}\equiv\text{N} < \text{Br–C}\equiv\text{N} < \text{PC–C}\equiv\text{N} < \text{P}\equiv\text{N} < \text{HS–C}\equiv\text{N} < \text{SiH}_3\text{–C}\equiv\text{N} < \text{HO–C}\equiv\text{N} < \text{CH}_3\text{–C}\equiv\text{N} < \text{Na–C}\equiv\text{N}$. The trend is persistent with the corresponding 0.0015- and 0.002-au mapped $V_{s,\min}$ for the monomers. This is also in agreement with the MP2(full) 0.001 au mapped $V_{s,\min}$, but somewhat in disagreement with the corresponding 0.0015- and 0.002-au mapped $V_{s,\min}$, as in the latter two mapped surfaces, the positions between ClCN and PCCN are inverted, that is, $\text{NC–C}\equiv\text{N} < \text{CN–C}\equiv\text{N} < \text{CCl}_3\text{–C}\equiv\text{N} < \text{F–C}\equiv\text{N} < \text{PC–C}\equiv\text{N} < \text{Cl–C}\equiv\text{N} < \text{Br–C}\equiv\text{N} < \text{P}\equiv\text{N} < \text{HS–C}\equiv\text{N} < \text{SiH}_3\text{–C}\equiv\text{N} < \text{HO–C}\equiv\text{N} < \text{CH}_3\text{–C}\equiv\text{N} < \text{Na–C}\equiv\text{N}$. Figure 3 illustrates the relationship between the nitrogen $V_{s,\min}$ in RN and the ΔE for the $\text{R–N}\cdots\text{Cl–CH}_3$ complexes.

3.3.3 Atomic charges

According to the recent studies of Grabowski^{33a} and McDowell et al,^{32d,33b} electronic charge is an important property of atoms in molecules. The amount of charge transfer Δq from Lewis base to Lewis acid can be an approximate descriptor of the strength of an intermolecular interaction, again this is independent of whether the charges are derived from the natural population analysis or from the QTAIM population analysis.^{33a} As McDowell noted,^{33b} the displacement of electronic charges on atoms in monomers gives an indication of complex formation. In addition, this displacement also explains certain geometrical and frequency changes. Although an exploration of the detail of this specific property is not the main purpose of this work, we only note that we observed such charge displacements upon formation of the $\text{RN}\cdots\text{Cl–CH}_3$ complexes, in which cases, the magnitudes of both the chlorine and nitrogen partial charges computed with the MP2(full)/6–311++G(3d,2p) method decrease with respect to that found for the corresponding atoms in the monomers. Figure 4 shows that the integrated QTAIM charges (for q , see eqn. 4) on the bonded chlorine and nitrogen atoms are both negative for each complex (i.e., $\text{Cl}^{\delta-}\cdots\text{N}^{\delta-}$), a feature which is also common for all the other complexes in the series. This may be physically meaningful

since the magnitude of the negative charge on the chlorine atom is substantially smaller than that on the other atom in the bonded pair, which is indeed essentially required for the realistic description of an acid-base interaction.³⁴

The transfer of charge between the binding partners in $\text{RN}\cdots\text{Cl}-\text{CH}_3$ is very marginal, all $< 0.0076 e$, which is probably an extreme form of polarization.

3.3.4 Natural bond orbital analysis

The molecular electrostatic surface potential analysis unequivocally demands that the $\text{N}\cdots\text{Cl}$ intermolecular interactions in the $\text{RN}\cdots\text{Cl}-\text{CH}_3$ complexes are the result of the overlap between the negative- and positive-areas of the electrostatic potential associated with the electron-donor and -acceptor atoms of the monomers. However, it does not explain the nature of the electron delocalization between the donor- and acceptor-orbitals involved. In an attempt to get some insight into this particular feature, NBO results¹³ of various important atomic- and molecular-orbitals involved between the monomers in the complexes are analyzed. It is found that the $\text{RN}\cdots\text{Cl}-\text{CH}_3$ complexes are stabilized by some charge transfer delocalization processes operating predominantly between electron-donor and -acceptor orbitals of the monomers. Two such predominant charge transfer channels identified in each of the $\text{RN}\cdots\text{Cl}-\text{CH}_3$ complexes are: one from the nitrogen lone-pairs n associated with the $V_{s,\text{min}}$ in RN to the $\sigma^*(\text{C}-\text{Cl})$ anti-bonding vacant orbital in $\text{Cl}-\text{CH}_3$, while the other from the $\sigma(\text{C}-\text{Cl})$ bonding orbital in $\text{Cl}-\text{CH}_3$ to a near-lying Rydberg-type RY^* N orbital in RN. In addition, there are a number of other ancillary electron-acceptor and -donor orbitals of the monomers which participate weakly upon the formation of the $\text{RN}\cdots\text{Cl}-\text{CH}_3$ complexes. To give an example, let us consider the $\text{HSCN}\cdots\text{Cl}-\text{CH}_3$ and $\text{CCl}_3\text{CN}\cdots\text{Cl}-\text{CH}_3$ complexes. In this former complex, $E^{(2)}$, eqn. 3, for $n(\text{N}) \rightarrow \sigma^*(\text{C}-\text{Cl})$, $\sigma(\text{C}-\text{Cl}) \rightarrow \text{RY}^*(\text{N})$, $n(\text{Cl}) \rightarrow \text{RY}^*(\text{N})$, $n(\text{Cl}) \rightarrow \sigma^*(\text{C}-\text{N})$, $n(\text{Cl}) \rightarrow \pi^*(\text{C}-\text{N})$, and $\sigma(\text{C}-\text{N}) \rightarrow \text{RY}^*(\text{Cl})$ are ca. 0.54, 0.75, 0.11, 0.18, 0.08, and 0.11 kcal mol^{-1} , respectively. Similarly, in the latter complex, $E^{(2)}$ is ca. 0.54, 0.75, 0.12, 0.25, 0.10, and 0.14 kcal mol^{-1} for the corresponding interactions, respectively. $E^{(2)}$ in all the other complexes are ranging roughly between 0.51 and 0.75 kcal mol^{-1} for $n(\text{N}) \rightarrow \sigma^*(\text{C}-\text{Cl})$ and that between 0.50 and 1.12 kcal mol^{-1} for $\sigma(\text{C}-\text{Cl}) \rightarrow \text{RY}^*(\text{N})$.

3.3.5 Vibrational characteristics

A feature commonly referred experimentally and theoretically to elicit the nature of a $\text{D}\cdots\text{H}-\text{A}$ hydrogen-bonded interaction lies in the length of the $\text{A}-\text{H}$ covalent bond that usually increases (or decreases). Concomitant to this increase (or decrease) there is generally a red-shift (or a blue-shift) in the infrared stretching vibrational frequency ω , and an increase (or a decrease) in the infrared intensity I ; the changes are with respect to the corresponding properties of the isolated molecule. The

aforementioned vibrational signatures are quite distinctly catalogued for the hydrogen-bonds,³⁵ but such attributes are yet to be formulated for halogen and other σ -hole interactions. For instance, the IUPAC recently proposed a more formal rule,²⁹ wherein it is accentuated that the infrared absorption and Raman scattering observables of both A–X and covalently bonded D in the D \cdots X–A motif are to be affected by halogen-bond formation. However, this does not vivify the typical nature of the spectral shift in the A–X bond vibrational stretching frequency that accompanies halogen-bond formation.

Notwithstanding, the chlorine bonded complexes examined in this study display a variability in the nature of the spectral shift associated with the C–Cl bond normal mode vibrational frequencies. This is evident of the data in Table 3. An inspection of this reveals that the relatively stable (although very weak) complexes of Cl–CH₃ with FCN, NCCN, NCNC, CCl₃CN, CH₃CN, SiH₃N, and PN are to be accompanied with vibrational red-shifts in the C–Cl stretching frequencies. And, those which are having relatively weak binding energies (i.e., H₃C–Cl complexes of ClCN, BrCN, HSCN, HOCN, PCCN, and NaCN) are to be tied up with vibrational blue-shifts in the stretching frequencies of the corresponding bonds. The red- and blue-shifts are in consistent with the elongation and contraction of the corresponding C–Cl bond lengths, respectively. There is an exception in which the CCl₃CN \cdots Cl–H₃C complex exhibits a characteristic red-shift in the C–Cl stretching frequency (though very small, $\Delta\omega = -0.08 \text{ cm}^{-1}$) and concomitant contraction of the C–Cl bond distance ($\Delta r(\text{C–Cl}) = -0.00018 \text{ \AA}$). The infrared intensity for the C–Cl vibrational band decreases for all cases irrespective of the nature of the substituents involved in the –R part of the monomers in the complexes. Figure 5a depicts the desired MP2(full) relationship between vibrational frequency shifts $\Delta\omega$ and bond length changes $\Delta r(\text{C–Cl})$ for the RN \cdots Cl–CH₃ complexes. Figure 5b illustrates the MP2(full) relationship between the decrease in the infrared intensity ΔI and the change in the integrated QTAIM charge $\Delta q(\text{Cl})$ associated with the chlorine of the CH₃–Cl monomer in the R–N \cdots Cl–CH₃ complexes.

3.3.6 Dipole moment changes

Electric dipole moment μ is a measurable physical property of a polar molecule. We have included the μ values in Table 1, which shows that the isolated molecules other than cyanogen (NCCN) are having permanent electric dipole moments, calculated using eqn. 4, meaning that they are all polar. The direction of dipole moment vector, $\vec{\mu}$, in isolated CH₃–Cl is from the partially negative chlorine towards the partially positive carbon. In the Lewis bases, the nitrogen is the most electronegative atom due to its very high negative charge, thus $\vec{\mu}$ in them each is directed from the nitrogen towards the center of the most electropositive site along or off the internuclear axis, as expected. Figure 6 illustrates the relationship between μ and $V_{s,\text{min}}$ showing that the latter property is probably a factor that determines the polarity of the monomers, a relationship that came to sight for the first time.

For the $\text{RN}\cdots\text{Cl}-\text{CH}_3$ complexes, the μ values are ranging from the least of 0.44 D for $\text{FCN}\cdots\text{Cl}-\text{CH}_3$ to the largest of 10.08 D for $\text{NaCN}\cdots\text{Cl}-\text{CH}_3$ with CCSD, in agreement with the MP2(full). In this comparison, the MP2(full) dipole moment of 0.47 D for the $\text{CCl}_3\text{CN}\cdots\text{Cl}-\text{CH}_3$ complex is not included as its geometry was not energy-minimized with CCSD. Nevertheless, both the methods display a substantial decrease in the dipole moments upon the formation of the $\text{RN}\cdots\text{Cl}-\text{CH}_3$ complexes, $\Delta\mu$, relative to the sum of the monomer dipole moment values (see Tables 1 and 3 for details). The specific feature is in contrast to what is normally observed for analogous complexes in the gas phase.³⁶

3.3.7 QTAIM- and NCI-RDG-based characteristics

Application of QTAIM to explore the bonding topologies in chemical compounds is widespread.¹¹ Several indicators of this theory are generally examined to gain valuable insights into whether there are noncovalent interactions between monomers in complexes, and whether they can suitably describe the geometrical and energetical stabilities. The two most common indicators of this theory are the (3,-1) saddle point called 'bond critical point (bcp)' and the 'bond path' that connect the nuclei of two atoms in a bonded pair in molecules. The MP2(full)/6-311++G(3d,2p) molecular graphs emerged from application of this theory to the $\text{RN}\cdots\text{Cl}-\text{CH}_3$ bimolecular complexes are illustrated in Figure 2; similar molecular graphs are also obtainable with CCSD(T)/6-311++G(3d,2p)//CCSD/6-311++G(3d,2p). Evidently, each molecular graph is well described by several (3,-1) bcps painted in darkred point-like spheres, including the (3,-1) bcp at the $\text{N}\cdots\text{Cl}$ intermolecular bonding region. Because $\text{N}\cdots\text{Cl}$ bond path lengths are almost identical to the corresponding intermolecular distances of separation for these complexes, the $\text{N}\cdots\text{Cl}$ geometries are therefore minimally strained.

The abovementioned QTAIM bonding topologies are in excellent agreement with the NCI RDG s vs. $(\text{sign } \lambda_2)\rho$ plots (see Eq. 6). Figure 7 depicts the NCI RDG s vs. $(\text{sign } \lambda_2)\rho$ plots for some selected complexes, including the $\text{Cl}-\text{CH}_3$ complexes of FCN, BrCN, PN, and HOCN. In each of these plots the $\text{N}\cdots\text{Cl}$ interaction is reminiscent of the trough centering near around $\rho \cong 0.0075$ au, where $\lambda_2 < 0$. There is also another trough in each of these plots which is appearing on the right of $\rho \cong 0.0$ au, i.e., around 0.0040 au, where $\lambda_2 > 0$. Both these troughs with CCSD(T)/6-311++G(3d,2p)//CCSD/6-311++G(3d,2p) appear at lower densities around $\rho \cong 0.0047$ au and 0.0045 au, respectively. We expect this latter peak must be due to a related (secondary) interaction arising between the electron-accepting and -donating fragments of the monomers in the complexes, contributing constructively to the intermolecular charge densities at (3,-1) bcps. According to NCI-RDG, these sorts of troughs are revealed in the low density regions when there are non-trivial chances of dative bond formations between atomic basins in chemical systems. The RDG s = 0.5 au isosurfaces painted in green circular volumes in Figs. 7a', 7b', 7c' and 7c' are appearing in the intermolecular bonding regions between the chlorine and nitrogen atoms. They lie in

the plane perpendicular to the bond path directions, ratifying the presence of weak interactions in the $\text{RN}\cdots\text{Cl}-\text{CH}_3$ complexes.

The CCSD(T) [MP2(full)] electron density at the $\text{N}\cdots\text{Cl}$ bond critical point, ρ_b , varies between 0.0045 [0.0070] and 0.0056 [0.0085] au, while its Laplacian, $\nabla^2\rho_b$, varies between 0.0201 [0.0284] and 0.0237 [0.0327] au for all the binary complexes investigated. The lower values of ρ_b and $\nabla^2\rho_b$ with CCSD(T) are not very surprising because it predicts relatively longer $\text{N}\cdots\text{Cl}$ intermolecular bond distances. The positive $\nabla^2\rho_b$ ($\nabla^2\rho_b > 0$) is indicative of regions of charge depletion.¹¹ Figure 8, as an example, illustrates the MP2(full)/6-311++G(3d,2p) relief maps of $\nabla^2\rho_b$ for the $\text{PN}\cdots\text{Cl}-\text{CH}_3$ and $\text{SiH}_3\text{CN}\cdots\text{Cl}-\text{CH}_3$ complexes in the HCCI plane. It displays the regions of charge-depletion and -concentration ($\nabla^2\rho_b > 0$ and $\nabla^2\rho_b < 0$, respectively) in the two complexes.

The three curvatures commonly referred in QTAIM to interpret chemical bonding topologies at bcps are described by the three principal eigenvalues $\lambda_{i(i=1,2,3)}$ of the second derivative matrix of the $\rho(r)$. As listed in Table 4, the computed values of first two of them, which are due to the plane perpendicular to the bond path direction, are degenerate and negative, $\lambda_1 \cong \lambda_2 < 0$, similar to what was found previously for C-C σ -bond of ethane.^{11,37} The third eigenvalue λ_3 along the bond path is positive, $\lambda_3 > 0$. Interestingly, the former is in line one of the NCI-RDG signatures that commends that for interatomic regions with $\lambda_2 < 0$ and $\lambda_2 > 0$ one may encounter bonded and non-bonded (steric) interactions, respectively.¹²

The ellipticity ε_b ($\varepsilon_b = \lambda_1/\lambda_2 - 1$) is an unambiguous tool with which to assess whether a pair of two atomic basins in a molecule is singly, or doubly, or triply bonded. To give an example, the carbon-carbon bond has an ellipticity value of 0.23 in aromatic benzene, of 0.45 in ethylene, and of 0.0 in acetylene and ethane.^{11,37} Its value for the $\text{N}\cdots\text{Cl}$ bcps in the $\text{RN}\cdots\text{Cl}-\text{CH}_3$ systems is almost close to zero, suggestive of cylindrically symmetric σ interactions.

The potential energy density V_b at the $\text{N}\cdots\text{Cl}$ bcps is negative ($V_b < 0$), showing a stabilizing interaction. However, its magnitude is smaller than the local kinetic energy density G_b at the corresponding bcps, whence the total energy density H_b ($H_b = G_b + V_b$) is positive at the corresponding bcps (i.e., $H_b > 0$). Clearly, this, together with the low values of ρ_b , with $\lambda_3 > 0$, with $\nabla^2\rho_b > 0$, and with the low negative values of λ_2 , shows that the $\text{N}\cdots\text{Cl}$ bcps in $\text{RN}\cdots\text{Cl}-\text{CH}_3$ are mapping to closed-shell interactions.^{11,12}

An intriguing two-electron descriptor is called electron delocalization index (δ), Eq. 7. It is often invoked to measure the extent of electron pairs delocalized between a given pair of two atomic basins in molecules.³⁸⁻⁴⁰ The property has a strong resemblance with bond order, and is calculated using a procedure we adopted previously.^{3d,3f,39} Table 4 lists the CCSD(T) calculated $\delta(\Omega_{\text{Cl}},\Omega_{\text{N}})$ values for the $\text{N}\cdots\text{Cl}$ interactions, which are considerably much more smaller than unity for each complex. In the series, the $\delta(\Omega_{\text{Cl}},\Omega_{\text{N}})$ value is determined to be the smallest for $\text{FCN}\cdots\text{Cl}-\text{CH}_3$ and the largest for $\text{Na}-\text{C}\equiv\text{N}\cdots\text{Cl}-$

CH₃ (0.0616 vs. 0.0787) with MP2(full), while the CCSD(T) determined these to vary between 0.0407 (NC–C≡N⋯Cl–CH₃) and 0.0541 (Na–C≡N⋯Cl–CH₃). Clearly, there is some mismatch between the $\delta(\Omega_{\text{Cl}}, \Omega_{\text{N}})$ values predicted by the two methods, but both the methods demand that the monomers in the equilibrium complex geometries are noncovalently bonded. Figure 9 shows the dependence of $\delta(\Omega_{\text{Cl}}, \Omega_{\text{N}})$ on ρ_{b} , of λ_3 on ρ_{b} , of λ_2 on $\delta(\Omega_{\text{Cl}}, \Omega_{\text{N}})$, and of $\delta(\Omega_{\text{Cl}}, \Omega_{\text{N}})$ on $\nabla^2 \rho_{\text{b}}$ for the RN⋯Cl–CH₃ complexes. These simple relationships demonstrate that each of the topological parameters can be served as a measure of bond electron delocalization.

4. Summary

Several binary complexes of Cl–CH₃ with the RN series of thirteen monomers are theoretically studied to address what causes the chlorine in Cl–CH₃ to undergo long-range contact with the negative nitrogen center. Several notes worthy points that explain this and the formation the RN⋯Cl–CH₃ complexes are listed below:

(1) The present benchmark revealed that most of the double- ζ basis sets employed in conjunction with MP2(full), B3PW91, and M06–2X methods, which are not augmented with at least two sets of each of d- and p-polarization functions, are inadequate to describe the true nature of the chlorine's electrostatic surface potential in Cl–CH₃, on the 0.001 electrons/bohr³ isodensity envelope; they all predicted a negative $V_{\text{s,max}}$ along the outermost extension of C–Cl bond. However, when the triple- ζ basis sets of Pople type are employed the chlorine surface became consistently positive with MP2(full), except for the smallest basis set, 6–311G(d). Applications of the two recommended functionals, B3LYP and M06–2X, did not reproduce the MP2(full) results even for medium size basis sets, although an agreement between them all is found when double- and triple- ζ basis sets are augmented with both "++" and "2d and 2p"-polarization functions. These results advocate that the nature of the chlorine's electrostatic potential on the 0.001 electrons/bohr³ isodensity envelope to be both method and basis set dependent. In contrary, the lateral sides of the chlorine were always negative regardless of the nature of the correlated methods and basis sets employed. Thus the combination of both the former and latter results demonstrates an anisotropic electron density topology around the chlorine nucleus in Cl–CH₃, in agreement with the CCSD.

(2) The nature of the chlorine $V_{\text{s,max}}$ in Cl–CH₃ is also explored on the 0.0015- and 0.002-electrons/bohr³ isodensity envelopes. In all such instances, a positive surface of electrostatic potential ($V_{\text{s,max}} > 0$) is unveiled on the chlorine, localized along the outermost extension of the of C–Cl bond, confirming the 0.001 electrons/bohr³ isodensity mapped CCSD, MP2(full), B3PW91, and M06–2X results obtained with sufficiently large basis sets of Pople and Dunning types. Clearly, the various interpretations made in the past to justify the reliability of a negative σ -hole on the chlorine surface are misleading, which are simply consequences of computational artefacts. We therefore recommend to use at least

0.0015 (or 0.002) electrons/bohr³ isodensity envelope to perform MESP analysis for borderline cases to avoid shortcomings to be raised of the theory.

(3) We showed that the chlorine in Cl-CH₃ is adept at forming weak noncovalent interactions with the nitrogen in several monomers RN, where R = FC, ClC, BrC, CH₃C, HOC, HSC, PCC, P, CCl₃C, SiH₃C, NCC, CNC, and NaC. These interactions are indeed resulted when the a positive $V_{s,max}$ on the chlorine in Cl-CH₃ is linked with the negative $V_{s,min}$ of the nitrogen in RN. The N \cdots Cl intermolecular bond distances of separation in the resulting complexes are ranging between 3.1520 and 3.2055 Å, which are each less than the sum of the chlorine and nitrogen van der Waals radii, 3.48 Å. The intermolecular bond angles, $\angle R=N\cdots Cl$ or $\angle N\cdots Cl-C$, are nearly linear for most of the complexes, revealing the directional nature of the chlorine's σ -hole. These are typical of σ -hole bonded interactions.

(4) The RN \cdots Cl-CH₃ complexes examined are having very weak binding energies, varying between -0.39 and -1.29 kcal mol⁻¹ with MP2(full). The CCSD(T) estimated binding energies for the corresponding complexes are substantially smaller. The energies for the most stable complexes of the series (e.g., NCCN \cdots Cl-CH₃ and CCl₃CN \cdots Cl-CH₃, etc) are comparable with that of the previously reported H₂C=O \cdots Cl-CH₃ complex, showing identical intermolecular bonding topologies.

(5) The BSSE for wave function methods may not be recommended because it leads to an unphysical overestimation of the energy of attraction. For instance, an inclusion of it erratically causes the negative sign of the ΔE to become more positive for most of the binary complexes.

(6) The C-Cl bond vibrational stretching frequencies for the RN \cdots Cl-CH₃ complexes experience characteristic red- and blue-shifts relative to that of the monomer frequency, showing that the nature of the vibrational spectral shift is indeed controlled by the nature the -R portions of the monomers in the complexes. There were concomitant elongations and contractions of the corresponding C-Cl bond distances, respectively. As expected, we observed a relationship between bond distance changes and vibrational spectral shifts associated with the C-Cl bond for the complexes.

(7) We showed that there is a substantial decrease in the total electric dipole moments of the complexes compared to the sum of their corresponding monomer dipole moments. The decrease $\Delta\mu$ is also in line with the corresponding decrease in the infrared intensity of the C-Cl band for the complexes.

(8) We noted a linear relationship between $V_{s,min}$ and ΔE for the RN \cdots Cl-CH₃ complex series, showing the former is a measure of the N \cdots Cl bond stability.

(9) The QTAIM descriptors, such as the low δ and ρ_b values, $\lambda_2 < 0$, $\varepsilon_b \cong 0.0$, $\nabla^2\rho_b > 0$, and $H_b > 0$, at the N \cdots Cl bcps are all suggestive of closed-shell σ -hole bonding, in agreement with the results of the NCI-RDG and NBO analyses.

(10) The cross-correlations established between ρ_b , λ_2 , λ_3 , and $\delta(\Omega_{Cl}, \Omega_N)$ are the characteristics of the RN \cdots Cl-CH₃ complexes, showing each of these QTAIM descriptors may be a measure of the N \cdots Cl bond electron delocalization.

Acknowledgement: PRV is a recipient of the National Science Council Research Associateship of Taiwan and thanks to the Department of Chemistry of National Taiwan University for providing workspace to conduct daily research in theoretical and computational chemistry. BYJ thanks Center for Emerging Material and Advanced Devices, Center for Quantum Science and Engineering, and Center for Theoretical Sciences, National Taiwan University for partial financial supports.

References

- (a) A. C. Legon, *Angew. Chem. Int. Ed.* 1999, 38, 2686; (b) P. Metrangolo, H. Neukirch, T. Pilati, G. Resnati, *Acc. Chem. Res.*, 2005, 38, 386; (c) P. Politzer, P. Lane, M. C. Concha, Y. Ma, J. S. Murray, *J. Mol. Model.* 2007, 13, 305; (d) P. Metrangolo, G. Resnati, *Science* 2008, 321, 918; (e) T. Clark, M. Hennemann, J. S. Murray, P. Politzer, *J. Mol. Model.* 2007, 13, 291; (f) A. C. Legon, *Phys. Chem. Chem. Phys.* 2010, 12, 7736; (g) P. Politzer, J. S. Murray, T. Clark, *Phys. Chem. Chem. Phys.* 2010, 12, 7748; (h) F. Meyer, P. Dubois, *Cryst. Eng. Comm.* 2013, 15, 3058; (i) A. V. Jentzsch, D. Emery, J. Mareda, S. K. Nayak, P. Metrangolo, G. Resnati, N. Sakai, S. Matile, *Nat. Commun.* 2012, 3, 905; (j) A. Priimagi, G. Cavallo, P. Metrangolo, G. Resnati, *Acc. Chem. Res.*, 2013, 46, 2686; (k) A. Mukherjee, S. Tothadi, G. R. Desiraju, *Acc. Chem. Res.* 2014, <http://pubs.acs.org/doi/abs/10.1021/ar5001555>; (l) P. Auffinger, F.A. Hays, E. Westhof, P. Shing Ho, *Proc. Natl. Acad. Sci. U S A* 2004, 101, 16789.
- (a) T. Brinck, J. S. Murray, P. Politzer, *Int. J. Quantum Chem.* 1992, 19, 57; (b) T. Brinck, J. S. Murray, P. Politzer, *Int. J. Quantum Chem.* 1993, 48, 73; (c) J. S. Murray, K. Paulsen, P. Politzer, *Indian Acad. Sci. (Chem. Sci.)* 1994, 106, 267. This article is available via DIALOG: <http://www.dtic.mil/dtic/tr/fulltext/u2/a274612.pdf>; (d) B. Bankiewicz, M. Palusiak, *Struct. Chem.* 2013, 24, 1297; (e) J. S. Murray, P. Politzer, *Theor. Chem. Acc.* 2012, 131, 1114; (f) K. E. Riley, J. S. Murray, P. Politzer, M. C. Concha, P. Hobza, *J. Chem. Theory Comput.* 2009, 5, 155; (g) G. R. Desiraju, P. Shing Ho, L. Kloo, A. C. Legon, R. Marquardt, P. Metrangolo, P. Politzer, G. Resnati, K. Rissanen, *Pure Appl. Chem.* 2013, 85, 1711.
- (a) P. Politzer, J. S. Murray, *Chem. Phys. Chem.* 2013, 14, 278; (b) P. Politzer, J. S. Murray, G. V. Janjic, S. D. Zaric, *Crystal* 2014, 4, 12; (c) A. Bauzá, T. J. Mooibroek, A. Frontera, *Angew. Chem. Int. Ed.* 2013, 18, 12317; (d) P. R. Varadwaj, A. Varadwaj, B. -Y. Jin, *Phys. Chem. Chem. Phys.* 2014, DOI: 10.1039/C4CP01775G; (e) S. A. C. McDowell, J. A. Joseph, *Phys. Chem. Chem. Phys.* 2014, 16, 10854; (f) P. R. Varadwaj, A. Varadwaj, B. -Y. Jin (ms submitted).
- (a) P. Politzer, K. E. Riley, F. A. Bulat, J. S. Murray, *Comput. Theor. Chem.* 2012, 2, 998; (b) J. S. Murray, P. Lane, P. Politzer, *J. Mol. Model.* 2009, 15, 2009, 723; (c) J. S. Murray, P. Politzer, *WIREs Comput. Mol. Sci.: Overview* 2011, 1, 153; (d) P. Politzer, J. S. Murray, T. Clark, *Phys. Chem. Chem. Phys.* 2013, 15, 11178.
- (a) P. Politzer, J. S. Murray, An Overview of σ -Hole Bonding, an Important and Widely-Occurring Noncovalent Interaction, Chapter 6, in: J. Leszczynski and M.K. Shukla (eds.), *Practical Aspects of*

- Computational Chemistry, DOI: 10.1007/978-90-481-2687-3_6, Springer Science Business Media B.V. 2009; (b) K. E. Riley, P. Hobza, *J. Chem. Theory Comput.* 2008, 4, 232; (c) K. Eskandari, H. Zariny, *Chem. Phys. Lett.* 2010, 492, 9; (d) X. Ding, M. Tuikka, M. Haukka, *Halogen Bonding in Crystal Engineering*, Ch 7, in: *Recent Advances in Crystallography*, Ed. J. B. Benedict, ISBN 978-953-51-0754-5, 312 pages, Publisher: InTech, 2012. This is available via DIALOG: <http://dx.doi.org/10.5772/48592>; (e) O. V. Shishkin, R. I. Zubatyuk, V. V. Dyakonenko, C. Lepetitcd, R. Chauvin, *Phys. Chem. Chem. Phys.* 2011, 13, 6837; (f) M. A. A. Ibrahim, *J. Mol. Model.* 2012, 18, 4625 (g) T. Clark, *WIREs Comput. Mol. Sci.* 2013, 3, 13; (h) J. S. Murray, L. Macaveiua, P. Politzer, *J. Comput. Sci.* (2014), <http://dx.doi.org/10.1016/j.jocs.2014.01.002>.
6. (a) J. P. M. Lommerse, A. J. Stone, R. Taylor, F. H. Allen, *J. Am. Chem. Soc.* 1996, 3108; (b) K. Dyduch, M. P. Mitoraj, A. Michalak, *J. Mol. Model.* 2013, 19, 2747; (c) M. Palusiak, *J. Mol. Struct: THEOCHEM* 2010, 945, 89.
7. (a) A. L. Allred, *Inorg. Nucl. Chem.* 17, 1961, 215; (b) D. R. Lide, *Handbook of Chemistry and Physics*, (87th ed.), Taylor & Francis, Boca Raton, FL (2006).
8. (a) Hazardous substance fact sheet, <http://nj.gov/health/eoh/rtkweb/documents/fs/1235.pdf>; (b) <https://www.osha.gov/Publications/osh3144.pdf>; (c) T. Umezawa, A. K. Baker, D. Oram, C. Sauvage, D. O'Sullivan, A. Rauthe-Schöch, S. A. Montzka, A. Zahn, C. A. M. Brenninkmeijer, *J. Geophys. Res. Atmos.* 2014, 119, doi:10.1002/2013JD021396. This is also available via DIALOG: http://www.caribic-atmospheric.com/elib/rev/Umezawa_2014.pdf; (d) E. G. Rochow, *J. Am. Chem. Soc.* 1945, 67, 963; (e) J. L. Graham, T. Yamada, *Understanding the Science Behind How Methylene Chloride/Phenolic Chemical Paint Strippers Remove Coatings*, <http://www.serdp.org/Program-Areas/Weapons-Systems-and-Platforms/Surface-Engineering-and-Structural-Materials/Coating-Removal/WP-1680/WP-1680>; (f) A. H. Maulitz, F. C. Lightstone, Y. J. Zheng, T. C. Bruice, *Proc. Natl. Acad. Sci. USA* 1997, 94, 6591; (g) S. Canneaux, C. Hammaecher, T. Cours, F. Louis, M. Ribaucour, *J. Phys. Chem. A* 2012, 116, 4396; (h) R. P. Schwarzenbach, P. M. Gschwend, D. M. Imboden, *Environmental Organic Chemistry*, Wiley & Sons, Hoboken, New Jersey, US, 2003.
9. (a) W. A. Herrebout, B. J. Van der Veken, *J. Phys. Chem.* 1993, 97, 10622; (b) W. A. Herrebout, B. J. Van der Veken, J. R. Durig, *J. Mol. Struct.* 1995, 332, 231; (c) M. Goubet, P. Asselin, P. Soulard, B. Madebene, *J. Phys.Chem. A* 2013, 117, 12569.
10. (a) A. D. Becke, *J. Chem. Phys.* 1993, 98, 5648; (b) Y. Zhao, D. G. Truhlar, *Theor. Chem. Acc.* 2008, 120, 2008, 215; (c) M. Head-Gordon, T. Head-Gordon, *Chem. Phys. Lett.* 1994, 220, 122; (d) G. E. Scuseria, C. L. Janssen, and H. F. Schaefer III, *J. Chem. Phys.* 1988, 89, 7382; (e) A. Bauzá, I. Alkorta, A. Frontera, J. Elguero, *J. Chem. Theory Comput.* 2013, 9, 5201.
11. (a) R. F. W. Bader, *Atoms in Molecules - A Quantum Theory*, Oxford University Press, Oxford, 1990; (b) C. F. Matta, R. J. Boyd (Eds.), "The Quantum Theory of Atoms in Molecules: From Solid State to DNA and Drug Design", Wiley-VCH, Weinheim, 2010.

12. (a) E R. Johnson, S. Keinan, P. Mori-Sanchez, J. Contreras-Garcia, A J. Cohen, W. Yang, *J. Am. Chem. Soc.* 2010, 132, 6498; (b) J. R. Lane, J. Contreras-García, J. P. Piquemal, B. J. Miller, Henrik G. Kjaergaard, *J. Chem. Theory Comput.* 2013, 9, 3263–3266.
13. (a) F. Weinhold, C. Landis, *Valency and Bonding, A Natural Bond Orbital Donor-Acceptor Perspective*, Cambridge University Press, New York, 2005; (b) I. V. Alabugin, M. Manoharan, S. Peabody, F. Weinhold, *J. Am. Chem. Soc.* 2003, 125, 5973; (c) F. Weinhold, *J. Comput. Chem.* 2012, 33, 2363.
14. Gaussian 09, Revision A.02, M. J. Frisch and G. W. Trucks and H. B. Schlegel and G. E. Scuseria and M. A. Robb and J. R. Cheeseman and G. Scalmani and V. Barone and B. Mennucci and G. A. Petersson and H. Nakatsuji and M. Caricato and X. Li and H. P. Hratchian and A. F. Izmaylov and J. Bloino and G. Zheng and J. L. Sonnenberg and M. Hada and M. Ehara and K. Toyota and R. Fukuda and J. Hasegawa and M. Ishida and T. Nakajima and Y. Honda and O. Kitao and H. Nakai and T. Vreven and Montgomery, Jr., J. A. and J. E. Peralta and F. Ogliaro and M. Bearpark and J. J. Heyd and E. Brothers and K. N. Kudin and V. N. Staroverov and R. Kobayashi and J. Normand and K. Raghavachari and A. Rendell and J. C. Burant and S. S. Iyengar and J. Tomasi and M. Cossi and N. Rega and J. M. Millam and M. Klene and J. E. Knox and J. B. Cross and V. Bakken and C. Adamo and J. Jaramillo and R. Gomperts and R. E. Stratmann and O. Yazyev and A. J. Austin and R. Cammi and C. Pomelli and J. W. Ochterski and R. L. Martin and K. Morokuma and V. G. Zakrzewski and G. A. Voth and P. Salvador and J. J. Dannenberg and S. Dapprich and A. D. Daniels and Ö. Farkas and J. B. Foresman and J. V. Ortiz and J. Cioslowski and D. J. Fox, Gaussian, Inc., Wallingford CT, 2009.
15. (a) T. Lu, F. Chen, *J. Comp. Chem.* 2012, 33, 580; (b) T. Lu, F. Chen, *J. Mol. Graph. Model.* 2012, 38, 314.
16. J. W. Ochterski, *Vibational Analysis in Gaussian*, 1999. This is available via DIALOG: http://www.gaussian.com/g_whitepap/vib/vib.pdf
17. R. Dennington, T. Keith, J. Millam, *GaussView, Version 5, Semichem Inc., Shawnee Mission KS*, 2009.
18. T. A. Keith, *AIMAll (Demo Version 11.03.14)*, 2011. Available via DIALOG at: <http://im.tkgristmill.com>.
19. C. F. Matta, S. Sowlati-Hashjin, A. D. Bandrauk, *J. Phys. Chem. A* 2013, 117, 7468.
20. (a) R. F. W. Bader, M. E. Stephens, *J. Am. Chem. Soc.* 1975, 97, 7391; (b) X. Fradera, M. A. Austen, R. F. W. Bader, *J. Phys. Chem. A* 1999, 103, 304.
21. The experimental data of molecular structural, dipole moment, vibrational, and thermodynamic properties of all the monomers investigated in this study can be found in the NIST Computational Chemistry Comparison and Benchmark Database, NIST Standard Reference Database Number 101. Release 16a, August 2013, Editor: R. D. Johnson III. This is available via DIALOG: <http://cccbdb.nist.gov/>

22. K. H. Hellwege, A. M. Hellwege (eds.). Landolt-Bornstein: Group II: Volume 6 Molecular Constants from Microwave, Molecular Beam, and Electron Spin Resonance Spectroscopy Springer-Verlag. Berlin. 1974.
23. R. D. Nelson Jr., D. L. Lide Jr., A. A. Maryott, Selected Values of Electric Dipole Moments for Molecules in Gas Phase. National Standard Reference Data Series - National Bureau of Standards 10 (NSRDS-NBS10), 1967. The article is available via DIALOG: <http://www.nist.gov/data/nsrds/NSRDS-NBS-10.pdf>
24. M. C. L. Gerry, F. Stroh, M. Winnewisser, J. Mol. Spectrosc. 1990, 140, 147.
25. G. P. Srivastava, D. Kumar, J. Phys. B: At. Mol. Phys. 1976, 9, 651.
26. S. Brünken, Z. Yu, C. A. Gottlieb, M. C. McCarthy, P. Thaddeus, APJ 2009, 706, 1588.
27. D. Priem, J. Cosleou, J. Demaison, I. Merke, W. Stahl, W. Jerzembeck, H. Burger, J. Mol. Spectrosc. 1998, 191, 183.
28. S. Brünken, C. A. Gottlieb, M. C. McCarthy, P. Thaddeus, ApJ 2009, 697, 880.
29. J. S. Murray, P. Politzer, Croat. Chem. Acta 2009, 82, 267.
30. R. F. W. Bader, M. T. Carroll, J. R. Cheeseman, C. Chang, J. Am. Chem. Soc. 1987, 109, 7968.
31. S. Alvarez, Dalton Trans. 2013, 42, 8617.
32. (a) P. Jurečka, J. Černý, P. Hobza, D. R. Salahub, J. Comput. Chem. 2007, 28, 555; (b) D. Hugas, S. Simon, M. Duran, Chem. Phys. Lett. 386, 2004, 373; (c) S. A. C. McDowell, Chem. Phys. Lett. 2006, 424, 239; (d) S. A. C. McDowell, Chem. Phys. Lett., 2014, 598, 1.
33. (a) S. J. Grabowski, Phys. Chem. Chem. Phys. 2014, 16, 1824; (b) S. A. C. McDowell, J. A. Joseph, Phys. Chem. Chem. Phys. 2014, 16, 10854.
34. T. T. T. Bui, S. Dahaoui, C. Lecomte, G.R. Desiraju, E. Espinosa, Angew. Chem. Int. Ed. 2009, 48, 3838.
35. G. R. Desiraju, Angew. Chem. Int. Ed. 50, 2011, 52.
36. A. Karpfen, Struct. Bond. 2008 126, 1.
37. V.G Tsirelson, R. P. Ozerov, Electron Density and Bonding in Crystals: Principles, Theory and X-ray Diffraction Experiments in Solid State Physics and Chemistry, Taylor & Francis, 1996.
38. C. F. Matta, J. Hernández-Trujillo, J. Phys. Chem. A 2003, 107, 7496.
39. P. R. Varadwaj, H. M. Marques, Phys. Chem. Chem. Phys. 2010, 12, 2126.
40. C. L. Firme, O. A. C. Antunes, P. M. Esteves, Chem. Phys. Lett. 468, 2009, 129.

Figure 1: 0.001 au isodensity surface mapped molecular electrostatic surface potential of Cl-CH₃, obtained with MP2(full)/6-311++G(3d,2p). In (a) the chlorine atom is on the top, and in (b), the carbon atom of the methyl group is facing the viewer. Illustrated in (c) with arrows are the $V_{s,max}$ and $V_{s,min}$ values of the five maxima (tiny red circles) and the three minima (tiny blue circles), respectively, distributed on the surface of the molecule. The colored bar (in kcal mol⁻¹) marked with red, yellow, green, cyan and blue represent the various strengths of the electrostatic potential.

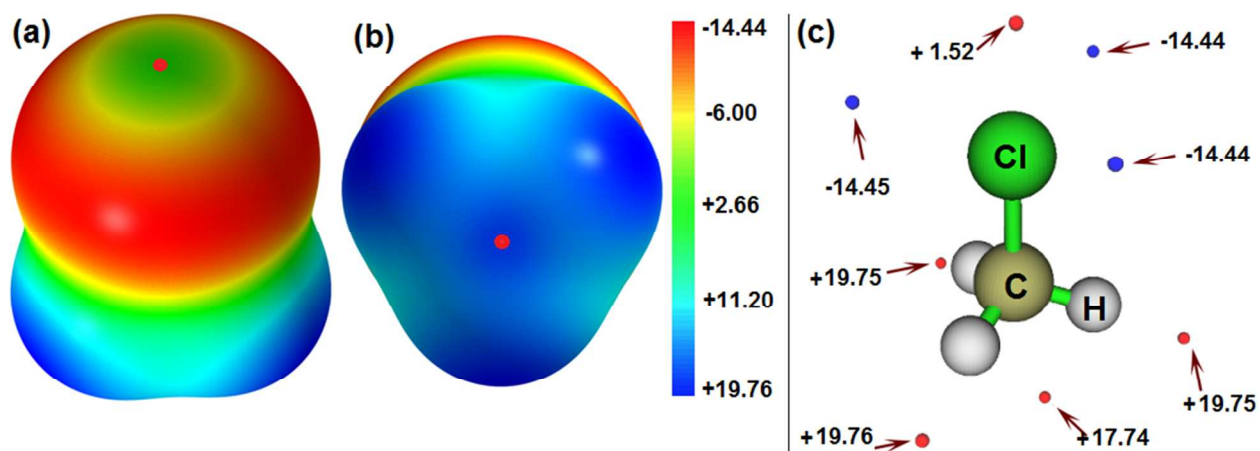


Figure 2: QTAIM molecular graphs for the σ -bonded complexes formed between the outer-end of the chlorine in $\text{CH}_3\text{-Cl}$ and the outer-end of the nitrogen in the $\text{R}\equiv\text{N}$ series of 13 monomers, where $\text{R} = \text{FC}, \text{ClC}, \text{BrC}, \text{CH}_3\text{C}, \text{HOC}, \text{HSC}, \text{PCC}, \text{P}, \text{CCl}_3\text{C}, \text{SiH}_3\text{C}, \text{NCC}, \text{CNC},$ and NaC , obtained with MP2(full)/6-311++G(3d,2p). The H, C, N, F, O, S, P, Cl, Br, and Na atoms are painted as large spheres in white-gray, gray, blue, lime, yellow, orange, green, dark-red, and purple, respectively. The (3,-1) critical points are depicted as small spheres in dark-red. The quantum mechanical exchange channels of maximal electron density, the bond paths, each connecting a pair two bonded atomic basins, are painted as lines in atom color. The bond paths in solid and dotted lines represent to shared- and closed-shell interactions. Atomic labeling is randomly shown.

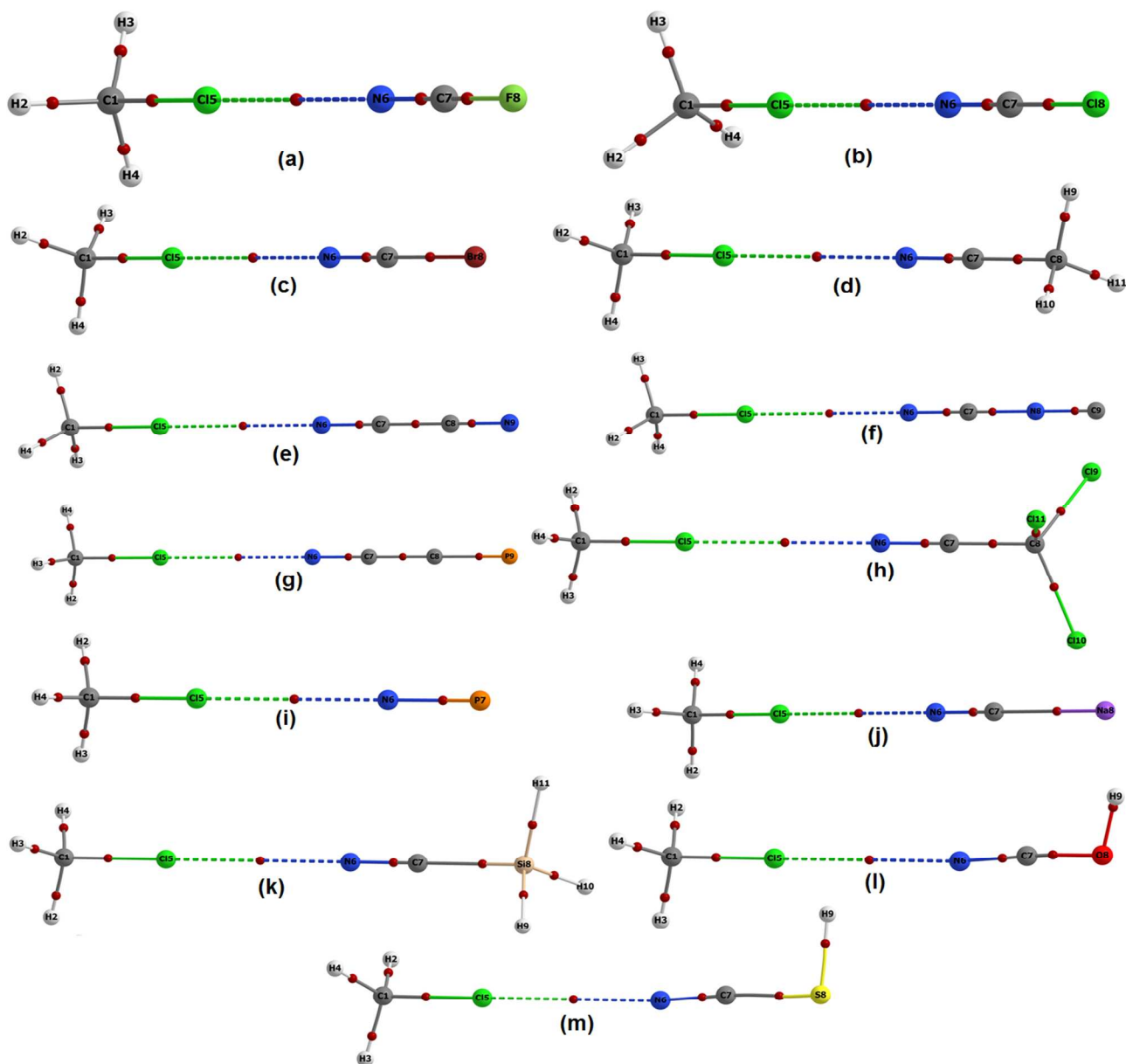


Figure 3: MP2(full)/6-311++G(3d,2p) dependence of binding energy on the nitrogen $V_{s,\min}$ for the $RN\cdots Cl-CH_3$ complexes (a), where $RN = FCN, ClCN, BrCN, CH_3CN, HOCN, NCCN, CNCN, CCl_3CN, HSCN, PCCN, PN, SiH_3CN,$ and $NaCN$. The corresponding CCSD/6-311++G(3d,2p) dependence is shown in (b) and (c), but in this case, the data for complex of CH_3Cl with CCl_3CN is excluded. In all the cases, the data are fitted to a linear function, and the adjusted-square regression coefficients, R^2 , are shown.

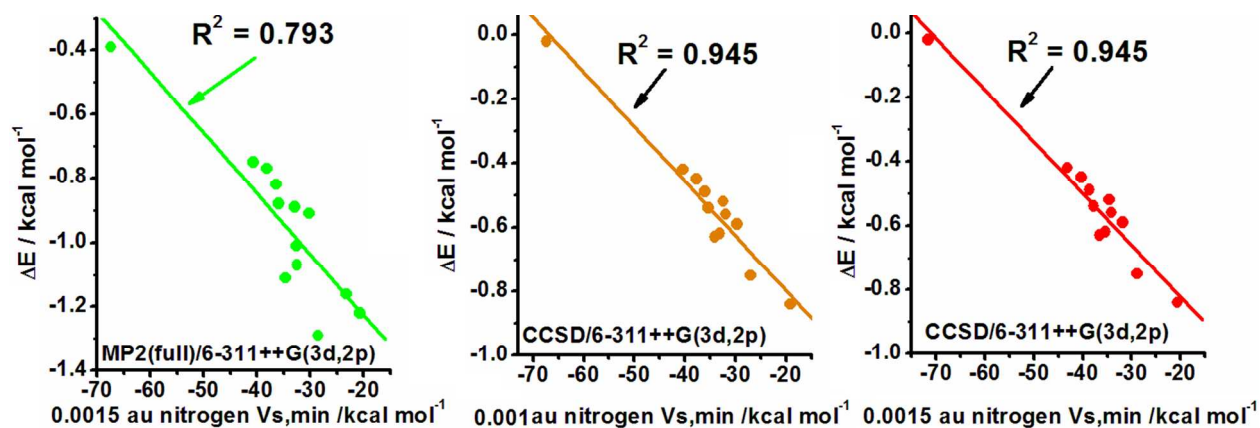


Figure 4: QTAIM integrated charges (in e) for the three randomly selected complexes of $\text{RN}\cdots\text{Cl}-\text{CH}_3$, computed with MP2(full)/6-311++G(3d,2p), where $\text{RN} = \text{FCN}$ (a), PN (b), and SiH_3CN (c). The integration error is roughly within ± 0.0005 e for all cases. Solid- and dotted-lines in orange represent the shared- and closed-shell interactions.

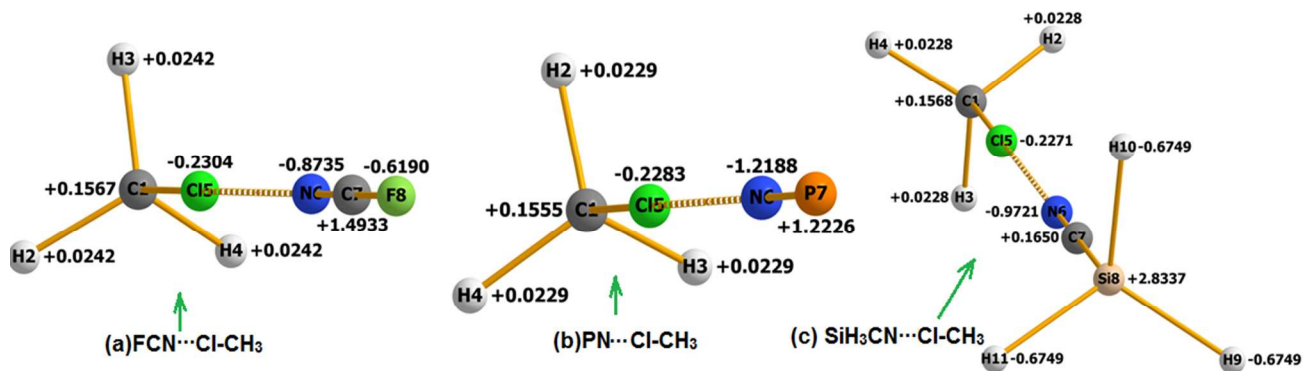


Figure 5: MP2(full)/6-311++G(3d,2p) relationship between the change in the C-Cl vibrational frequency $\Delta\omega$ and the change in the C-Cl bond length Δr for the $\text{RN}\cdots\text{Cl}-\text{CH}_3$ complexes, where $\text{RN} = \text{FCN}, \text{ClCN}, \text{BrCN}, \text{CH}_3\text{CN}, \text{HOCN}, \text{HSCN}, \text{PCCN}, \text{PN}, \text{CCl}_3\text{CN}, \text{SiH}_3\text{CN}, \text{NCCN}, \text{CNCN},$ and NaCN . Shown in (b) is the relationship between the change in the C-Cl infrared band intensity ΔI and the change in the integrated charge of the chlorine atom Δq for the corresponding complexes. The data are fitted to a linear function, and the adjusted-square regression coefficient, R^2 , is shown for each case.

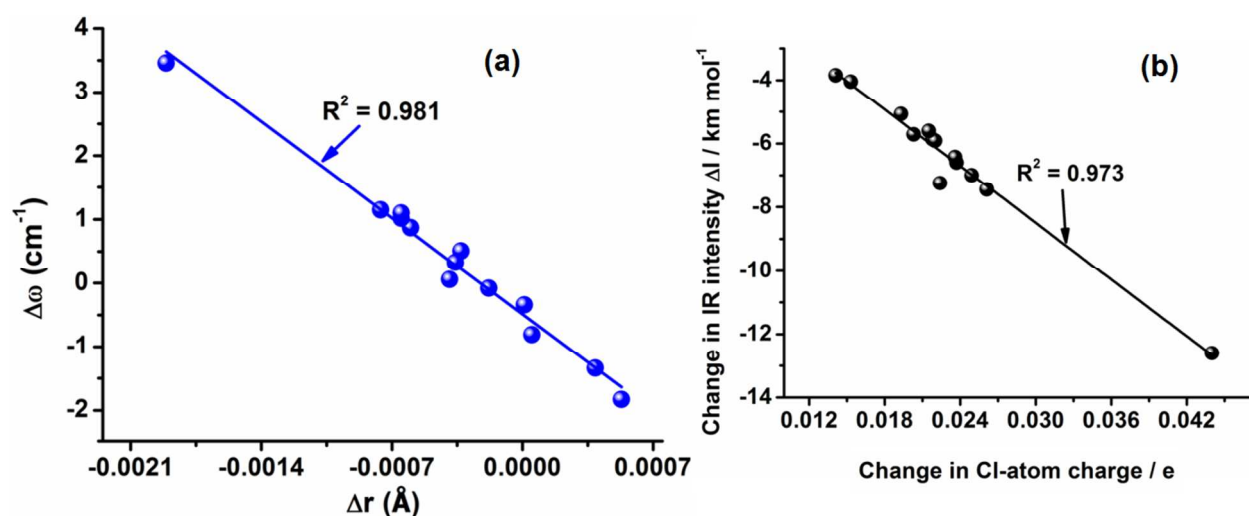


Figure 6: (a) MP2(full)/6-311++G(3d,2p) relationship between electric dipole moments μ and the 0.0015 au mapped nitrogen negative areas of the electrostatic potential $V_{s,\min}$ along the outermost extensions of the RN bonds for the thirteen monomers in the $\text{RN}\cdots\text{Cl}-\text{CH}_3$ complexes, where $R = \text{FC}, \text{ClC}, \text{BrC}, \text{CH}_3\text{C}, \text{HOC}, \text{HSC}, \text{PCC}, \text{P}, \text{CCl}_3\text{C}, \text{SiH}_3\text{C}, \text{NCC}, \text{CNC},$ and NaC . In (b), the corresponding CCSD/6-311++G(3d,2p) relationship is displayed.

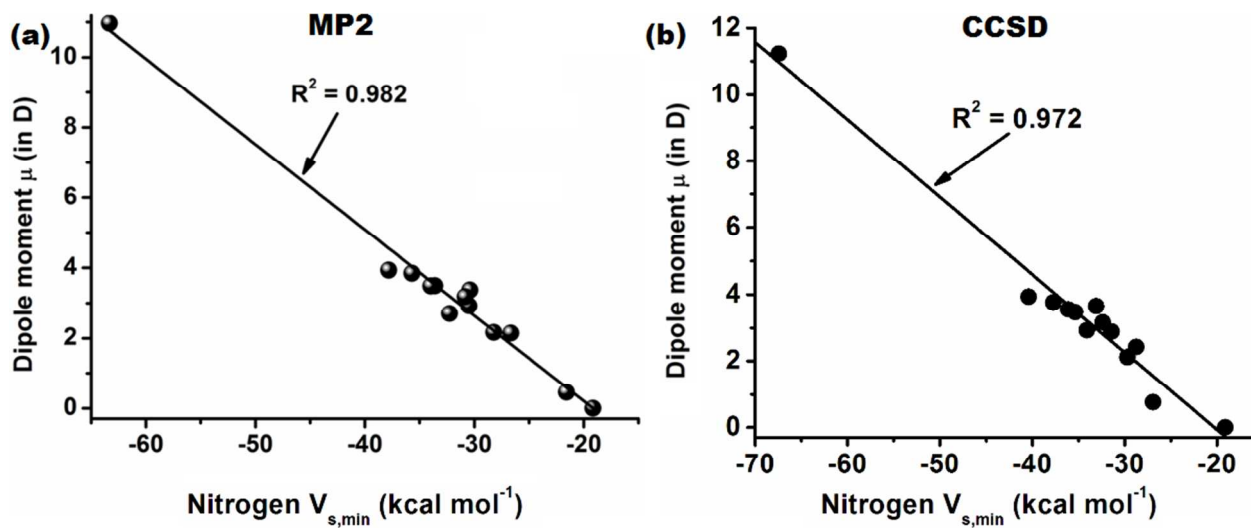


Figure 7: Examples showing the NCI RDG s vs. $\text{sign}(\lambda_2)\rho$ plots for four selected binary complexes formed between the positive σ -hole of the chlorine in CH_3Cl and the outer end of the nitrogen in FCN (a), BrCN (b), PN (c) and HOCN (d), respectively, obtained using $\text{MP2}(\text{full})/6\text{-}311++\text{G}(3\text{d},2\text{p})$. Depicted in (a'), (b'), (c') and (d') are the RDG $s = 0.5$ au isosurfaces painted in green circular volumes for the corresponding complexes, respectively. The troughs in the regions $0.0080 < \rho < 0.0090$ au, as well as the isosurfaces painted in green circular volumes, are reminiscent of noncovalent interactions in these complexes.

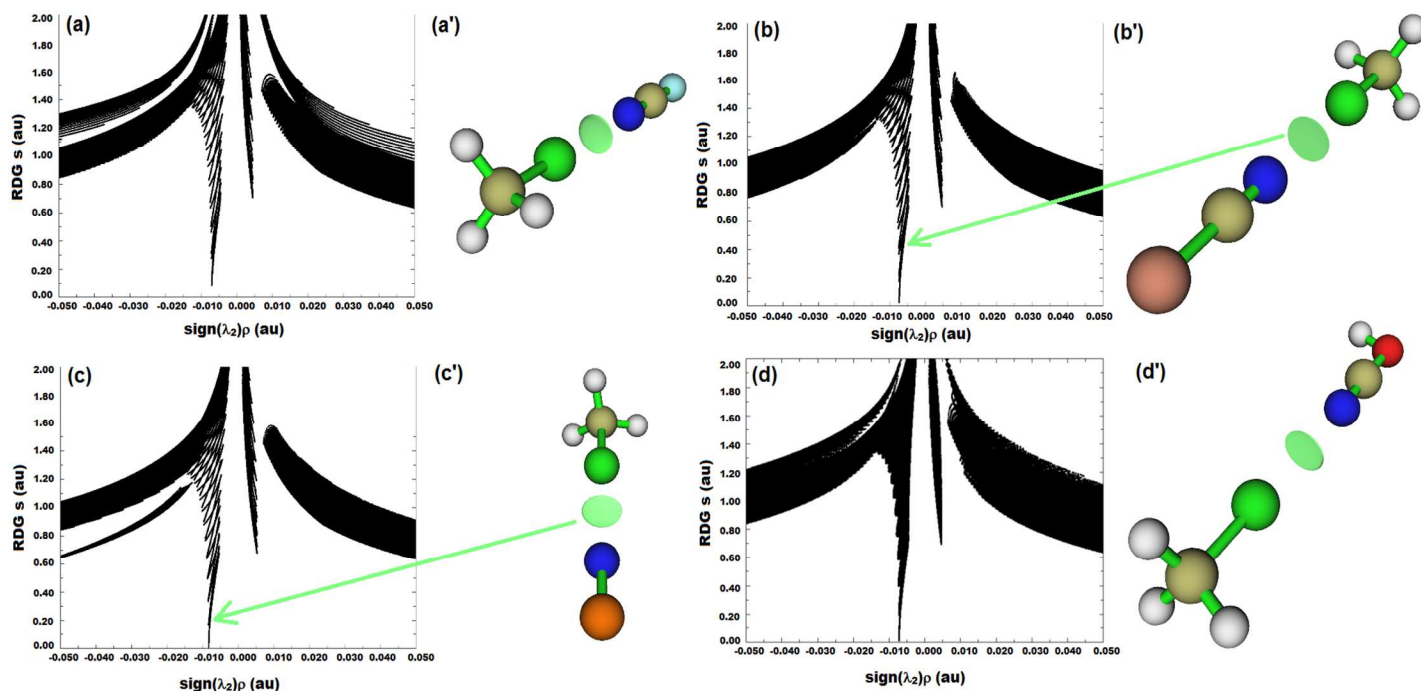


Figure 8: An example displaying the MP2(full)/6-311++G(3d,2p) relief maps of the Laplacian of the charge density for the $\text{P}\equiv\text{N}\cdots\text{Cl}-\text{CH}_3$ (a) and $\text{SiH}_3\text{C}\equiv\text{N}\cdots\text{Cl}-\text{CH}_3$ (b) complexes in the HCl plane (heights truncated at 7 au). The H atom in $\text{Cl}-\text{CH}_3$ facing the viewer is cloaked. The regions of charge depletion, and of charge concentration, are marked with arrows. Color ranges, in au ($1 \text{ au} = 24.099 \text{ e}\text{\AA}^{-5}$), are red (negative), less than -1.05 ; yellow, around -0.5 ; green, around $+0.03$; cyan, around $+0.5$, and blue (positive), less than $+1.2$. Shown in (c) and (d) are the 0.001 au isodensity isosurface mapped $\nabla^2\rho$ for isolated $\text{Cl}-\text{CH}_3$, revealing various regions of charge-depletion and -concentration. The $-\text{CH}_3$ and $-\text{Cl}$ groups in (c) and (d) are facing the viewer, respectively.

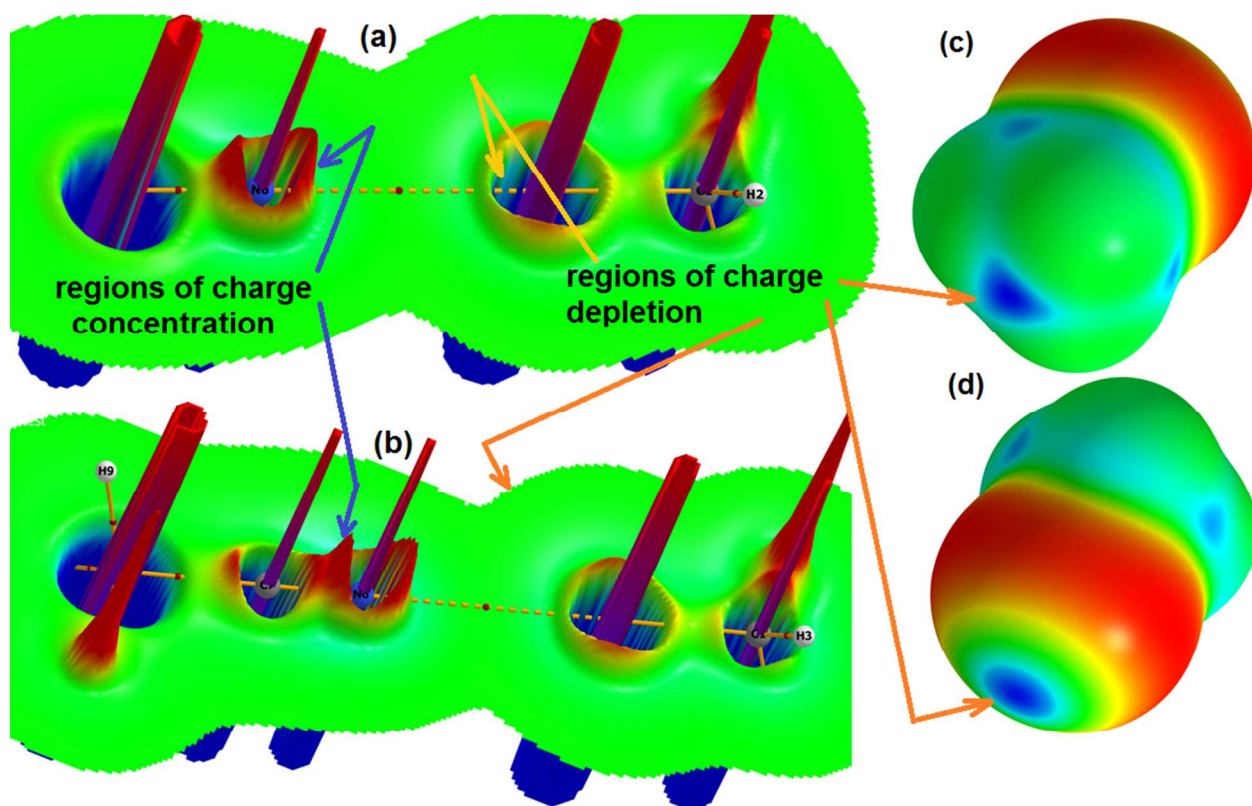


Figure 9: CCSD(T)/6-311++G(3d,2p)//CCSD/6-311++G(3d,2p) dependence of $\delta(\Omega_{Cl},\Omega_N)$ on ρ_b (a), of λ_3 on ρ_b (b), of λ_2 on $\delta(\Omega_{Cl},\Omega_N)$ (c), and of $\delta(\Omega_{Cl},\Omega_N)$ on $\nabla^2\rho_b$ (d) for the $RN\cdots Cl-CH_3$ complexes, where $R=N$ = FCN, ClCN, BrCN, CH_3CN , HOCN, HSCN, PCCN, PN, SiH_3CN , NCCN, CNCN, and NaCN. The data in each plot are fitted to a linear function, and the corresponding adjusted-square regression coefficient (R^2) is shown.

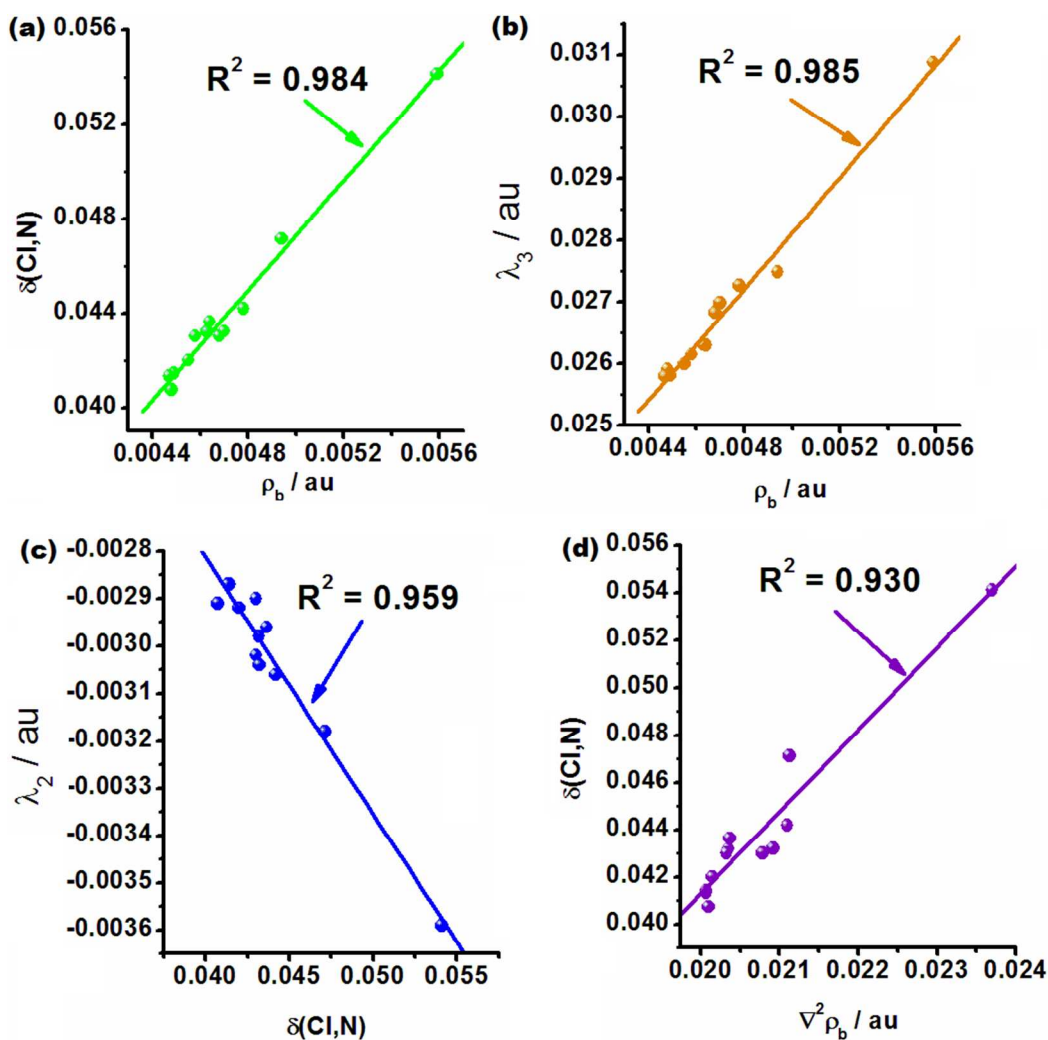


Table 1: Selected MP2(full)/6-311++G(3d,2p) predicted physical properties^a of the 14 isolated molecules. Each second line entry in parentheses represents the corresponding values computed with CCSD/6-311++G(3d,2p). The properties include the 0.001-, 0.0015-, and 0.002-au isodensity surfaces mapped local most minima of electrostatic surface potential $V_{s,\min}$ on the outer extensions of the RN bonds in the monomers, the zero-point vibrational energies ZPVE, the electric dipole moments μ , and the electron-acceptor and -donor bond distances r . Values of these properties are given in units of kcal mol⁻¹, kcal mol⁻¹, D, and Å, respectively. Experimental values of μ and ZPVE are included wherever available.

Monomer	$V_{s,\min}$ (0.001 au)	$V_{s,\min}$ (0.0015 au)	$V_{s,\min}$ (0.002 au)	μ	$\mu(\text{expt.})^{21-23}$	$r(\text{C-Cl})/r(\text{P-N})/r(\text{C-N})$	ZPVE	ZPVE(expt.) ²¹⁻²³
H ₃ CCl	---			1.906 (2.132)	1.87	1.7761 (1.7860)	24.3 (24.1)	23.0
NCCN	-19.16 (-19.09)	-20.68 (-20.62)	-21.76 (-21.72)	0.000 (0.000)	0.00	1.1740 (1.1564)	9.5 (10.0)	9.7
CNCN	-21.58 (-26.94)	-23.23 (-28.91)	-24.40 (-30.31)	0.457 (0.763)	0.71 ^a	1.1720 (1.1570)	9.4 (9.7)	---
CCl ₃ CN	-26.66 (-28.34)	-28.58 (-30.78)	-29.95 (-32.29)	2.148 (2.427)	1.78	1.1711 (1.1549)	10.8 (11.1)	---
FCN	-28.22 (-29.69)	-30.18 (-31.78)	-31.58 (-33.27)	2.167 (2.118)	2.17	1.1690 (1.1550)	6.1 (6.3)	6.1
ClCN	-30.48 (-31.93)	-32.61 (-34.17)	-34.10 (-35.76)	3.369 (2.881)	3.50	1.1797 (1.1571)	5.2 (5.4)	5.3
BrCN	-30.84 (-32.39)	-32.94 (-34.63)	-34.49 (-36.24)	3.179 (3.164)	2.94 ^b	1.1738 (1.1580)	4.8 (5.0)	4.9
PCCN	-30.39 (-33.09)	-32.51 (-35.32)	-34.02 (-36.95)	2.926 (3.657)	2.82	1.1725 (1.1610)	8.0 (8.4)	
PN	-32.26 (-34.10)	-34.67 (-36.63)	-36.42 (-38.49)	2.702 (2.924)	2.75	1.5195 (1.4894)	1.7 (2.0)	1.9
HSCN	-33.61 (-35.34)	-35.95 (-37.78)	-37.66 (-39.56)	3.492 (3.465)	--- ^c	1.1729 (1.1587)	10.4 (10.6)	---
SiH ₃ CN	-33.98 (-36.08)	-36.39 (-38.58)	-38.16 (-40.44)	3.487 (3.556)	3.44 ²⁷	1.1727 (1.1589)	20.8 (20.8)	---
HO-CN	-35.69 (-37.71)	-38.14 (-40.30)	-39.92 (-42.19)	3.841 (3.769)	--- ^d	1.1705 (1.1573)	13.3 (13.6)	12.4
CH ₃ CN	-37.82 (-40.37)	-40.67 (-43.13)	-42.41 (-45.18)	3.932 (3.937)	3.92	1.1679 (1.1553)	28.5 (28.6)	27.5
NaCN	-63.33 (-67.40)	-67.44 (-71.60)	-70.53 (-74.78)	10.971 (11.225)	---	1.1809 (1.1689)	3.8 (4.0)	---

^a Ref.²⁴

^b Ref.²⁵

^c *a*-type and *b*-type dipole moments along the two principal inertial axes were previously reported to be $\mu_a = 3.46$ D and $\mu_b = 1.09$ D, respectively, ref.²⁶

^d *a*-type and *b*-type dipole moments along the two principal inertial axes were previously reported to be $\mu_a = 3.7$ D and $\mu_b = 1.6$ D, respectively, ref.²⁸

Table 2: The 0.001 au isodensity surface mapped local most electrostatic potential $V_{s,\max}$ of the chlorine in Cl-CH_3 , along the outermost extension of the C-Cl bond, obtained from various levels of theory. ^{a,b} Values given in parentheses and square brackets correspond to the values obtained on the 0.0015- and 0.0020-au electron density isosurfaces, respectively.

Basis Set	MP2(full)	M06-2X	B3PW91
cc-pVDZ	-1.55 (+0.52)[+2.45]	-2.16(-0.14)[+1.76]	-1.80(+0.28)
aug-cc-pVDZ	-0.07(+2.35)[+4.68]	-0.50(+1.93)	-0.39(+2.03)
cc-pVTZ	-0.55(+1.80)[+3.95]	-1.39(+0.89)	-0.97(+1.32)
jul-cc-pV(D+d)Z	+0.46(+2.99)[+5.31]	+0.38(+2.93)	+0.45(+2.99)
Jul-cc-pV(T+d)Z	+0.76(+3.25)[+5.55]	+0.51(2.97)	+0.66(+3.14)
aug-cc-pVTZ	+0.59(+3.56)[+5.32]	+0.15(+2.57)	+0.32(+2.75)
6-31G(d)	-1.22(+1.11)[+3.80]	-1.52(+0.74)	-1.23(+1.05)
6-31G(d,p)	-0.73(+1.62)[+3.25]	-1.68(+0.56)	-1.35(+0.92)
6-31G(2d,p)	-0.05(+2.48)[+4.76]	+0.20(+2.74)	+0.38(+2.93)
6-31G(2d,2p)	+0.22(+2.77)[+5.07]	+0.24(+2.89)	+0.33(+2.89)
6-31+G(d,p)	-0.44(+2.10)[+4.40]	-1.32(+1.12)	-1.04(+1.42)
6-31++G(d,p)	-0.40(+2.14)[+4.45]	-1.29(+1.45)	-1.01(+1.41)
6-31++G(2d,p)	+0.28(+2.97)[+5.36]	+0.62(+3.36)	+0.69(+3.44)
6-31++G(2d,2p)	+1.54(+3.25)[+5.67]	+0.68(+3.43)	+0.65(+3.25)
6-311g(d)	-0.31(+2.14)[+4.34]	-1.12(+1.37)	-0.46(+1.95)
6-311G(d,p)	+0.49(+3.0)[+5.24]	-1.12(+1.25)	-0.54(+1.86)
6-311+G(d,p)	+1.17(+3.75)[+6.10]	-0.51(+1.93)	-0.08(+2.37)
6-311++G(d,p)	+1.10(+3.68)[+6.03]	-0.60(+1.84)	-0.17(+2.28)
6-311G(2d,p)	+1.37(+4.14)[+6.61]	+1.06(+3.85)	+1.44(+4.27)
6-311G(2d,2p)	+1.34(+4.14)[+6.61]	+1.01(+3.80)	+1.32(+4.11)
6-311+G(2d,2p)	+1.60(+4.38)[+6.84]	+1.31(+4.10)	+1.52(+4.27)
6-311++G(2d,2p)	+1.54(+4.31)[+6.77]	+1.24(+4.01)	+1.46(+4.20)
6-311++G(3d,2p)	+1.52(+4.07)[+6.35]	+1.38(+3.86)	+1.43(+3.87)
CCSD/6-311++G(3d,2p)	+1.01 (+3.59) [+5.96]		

^a Values in kcal mol⁻¹.

^b -0.73 and -1.38 kcal mol⁻¹ with B3PW91/aug-cc-pVDZ and B3PW91/6-31G(d,p), respectively, ref.^{5f} -0.9 kcal mol⁻¹ with B3PW91/6-311G(d), ref.^{5h} -1.5 kcal mol⁻¹ with B3PW91/6-31G(d,p), ref.^{1c} -2.1 kcal mol⁻¹ with RHF/6-31G(d)//RHF/STO-3G, ref.^{2a}

^c +3.96 and 2.90 kcal mol⁻¹ (0.002 au mapped) with B3PW91/aug-cc-pVDZ and B3PW91/6-31G(d,p), respectively.^{5f}

Table 3: Selected physical properties of the $\text{RN}\cdots\text{Cl}-\text{CH}_3$ binary complexes, where $\text{RN} = \text{FCN}, \text{ClCN}, \text{BrCN}, \text{CH}_3\text{CN}, \text{HOCN}, \text{HSCN}, \text{PCCN}, \text{PN}, \text{CCl}_3\text{CN}, \text{SiH}_3\text{CN}, \text{NCCN}, \text{CNCN}$, and NaCN , obtained using MP2(full)/6-311++G(3d,2p). The properties include the intermolecular bond distances ($r/\text{\AA}$), the uncorrected binding energies ($\Delta E/\text{kcal mol}^{-1}$, Eq. 2), the basis set superposition energies (BSSE/ kcal mol^{-1}), the differences in the zero-point vibrational energies ($\Delta\text{ZPVE}/\text{kcal mol}^{-1}$), the change in the dipole moments ($\Delta\mu/\text{D}$), the change in the C–Cl bond vibrational frequencies ($\Delta\omega/\text{cm}^{-1}$), the change in the C–Cl bond distances ($\Delta r(\text{C}-\text{Cl})/\text{\AA}$), and the change in the C–Cl infrared band intensities ($\Delta I/\text{km mol}^{-1}$).

Complex ^a	$r(\text{N}\cdots\text{Cl})^b$	$\Delta E^{c,d}$	BSSE	ΔZPVE^c	$\Delta\mu^{b,c}$	$\Delta\omega^c$	$\Delta r(\text{C}-\text{Cl})^{b,c}$	ΔI^c
$\text{FCN}\cdots\text{Cl}-\text{CH}_3$	3.2033 (3.3798)	-0.91 (-0.59)	0.82	0.279	-3.53 (-3.81)	-0.34	0.00001 (-0.00001)	-5.7
$\text{ClCN}\cdots\text{Cl}-\text{CH}_3$	3.1833 (3.3673)	-1.01 (-0.56)	0.92	0.257	-3.51 (-3.80)	+0.51	-0.00033 (-0.00104)	-5.9
$\text{BrCN}\cdots\text{Cl}-\text{CH}_3$	3.1916 (3.3824)	-0.89 (-0.52)	0.79	0.203	-3.52 (-3.83)	+0.33	-0.00036 (-0.00095)	-5.9
$\text{CH}_3\text{CN}\cdots\text{Cl}-\text{CH}_3$	3.2040 (3.3820)	-0.75 (-0.42)	0.78	0.244	-3.41 (-3.58)	+1.15	-0.00076 (-0.00140)	-7.5
$\text{NCCN}\cdots\text{Cl}-\text{CH}_3$	3.2002 (3.3809)	-1.22 (-0.84)	0.84	0.27	-0.15 (-0.08)	-1.34	0.00039 (-0.00015)	-3.8
$\text{CNCN}\cdots\text{Cl}-\text{CH}_3$	3.1981 (3.3820)	-1.16 (-0.75)	0.82	0.244	-1.09 (-2.44)	-1.83	0.00053 (0.00016)	-4.0
$\text{PCCN}\cdots\text{Cl}-\text{CH}_3$	3.1781 (3.3656)	-1.07 (-0.62)	0.89	0.238	-3.55 (-3.82)	+0.06	-0.00039 (-0.00112)	-5.6
$\text{CCl}_3\text{CN}\cdots\text{Cl}-\text{CH}_3^e$	3.1725	-1.29	1.09	0.256	-3.58	-0.08	-0.00018	-5.1
$\text{PN}\cdots\text{Cl}-\text{CH}_3$	3.1573 (3.3673)	-1.11 (-0.63)	0.89	0.255	-3.49 (-3.76)	-0.81	0.00005 (-0.00104)	-7.3
$\text{NaCN}\cdots\text{Cl}-\text{CH}_3$	3.1520 (3.3181)	-0.39 (-0.02)	0.85	0.251	-3.05 (-3.28)	+3.46	-0.00191 (-0.00293)	-12.6
$\text{SiH}_3\text{CN}\cdots\text{Cl}-\text{CH}_3$	3.2055 (3.3828)	-0.82 (-0.49)	0.79	0.235	-3.49 (-3.74)	+1.02	-0.00065 (-0.00120)	-6.4
$\text{HOCN}\cdots\text{Cl}-\text{CH}_3$	3.1983 (3.3776)	-0.77 (-0.45)	0.78	0.249	-3.16 (-3.31)	+1.10	-0.00065 (-0.00123)	-7.0
$\text{HSCN}\cdots\text{Cl}-\text{CH}_3$	3.1887 (3.3629)	-0.88 (-0.54)	0.83	0.240	-3.34 (-3.55)	+0.87	-0.00060 (-0.00095)	-6.6

^a See Figure 2 for geometric details.

^b CCSD/6-311++G(3d,2p) values are given in the parentheses.

^c $\Delta X = X(\text{complex}) - \sum X(\text{isolated})$, where the mathematical sum, \sum , is over the two monomers, and X can be any one of the properties, ZPVE, μ , ω , $r(\text{C}-\text{Cl})$, or I.

^d CCSD(T)/6-311++G(3d,2p)//CCSD/6-311++G(3d,2p) values are given in the parentheses.

^e This complex could not be energy-minimized because of g_write error of Gaussian 09.

Table 4: Selected topological properties^a for the RN \cdots Cl-CH₃ binary complexes, where RN = FCN, ClCN, BrCN, CH₃CN, HOCN, HSCN, PCCN, PN, SiH₃CN, NCCN, CNCN, and NaCN), obtained with CCSD(T)/6-311++G(3d,2p)//CCSD/6-311++G(3d,2p). Values are in au.^b

Complexes	ρ_b	λ_1	λ_2	λ_3	$\nabla^2\rho_b$	ε_b	V_b	G_b	H_b	$\delta(\Omega_{Cl}, \Omega_N)$
FCN \cdots Cl-CH ₃	0.00449	-0.00287	-0.00287	0.02581	0.02007	0.00	-0.00261	0.00382	0.00120	0.04145
ClCN \cdots Cl-CH ₃	0.00468	-0.00302	-0.00302	0.02683	0.02079	0.00	-0.00276	0.00398	0.00122	0.04302
BrCN \cdots Cl-CH ₃	0.00455	-0.00292	-0.00292	0.02600	0.02015	0.00	-0.00266	0.00385	0.00119	0.04201
CH ₃ CN \cdots Cl-CH ₃	0.00464	-0.00296	-0.00296	0.02630	0.02037	0.00	-0.00272	0.00390	0.00119	0.04364
NCCN \cdots Cl-CH ₃	0.00448	-0.00291	-0.00291	0.02592	0.02010	0.00	-0.00261	0.00382	0.00121	0.04075
CNCN \cdots Cl-CH ₃	0.00447	-0.00287	-0.00287	0.02580	0.02007	0.00	-0.00260	0.00381	0.00121	0.04134
PCCN \cdots Cl-CH ₃	0.00470	-0.00304	-0.00304	0.02699	0.02092	0.00	-0.00277	0.00400	0.00123	0.04322
PN \cdots Cl-CH ₃	0.00494	-0.00318	-0.00318	0.02749	0.02113	0.00	-0.00291	0.00409	0.00119	0.04714
NaCN \cdots Cl-CH ₃	0.00559	-0.00359	-0.00359	0.03088	0.02370	0.00	-0.00337	0.00465	0.00128	0.05412
SiH ₃ CN \cdots Cl-CH ₃	0.00463	-0.00298	-0.00298	0.02631	0.02035	0.00	-0.00272	0.00390	0.00119	0.04320
HOCN \cdots Cl-CH ₃	0.00458	-0.00292	-0.00290	0.02615	0.02033	0.01	-0.00267	0.00388	0.00120	0.04302
HSCN \cdots Cl-CH ₃	0.00478	-0.00310	-0.00306	0.02727	0.02110	0.01	-0.00282	0.00405	0.00123	0.04419

^a The properties include the charge density (ρ_b / au), the three eigenvalues of the Hessian of the charge density matrix ($\lambda_{i(i=1,2,3)}$ / au), the Laplacian of the charge density ($\nabla^2\rho_b$ / au), the ellipticity ($\varepsilon_b = \lambda_1/\lambda_2 - 1$), the potential energy density (V_b /au), the local kinetic energy density (G_b /au), the total energy density H_b ($H_b = (G_b + V_b)$ /au), and the electron delocalization index (δ).

^b1 au of $\rho_b = 6.7483 \text{ e}\text{\AA}^{-3}$; 1 au of $\lambda_{i(i=1,2,3)} = 24.099 \text{ e}\text{\AA}^{-5}$; 1 au of $\nabla^2\rho_b = 24.099 \text{ e}\text{\AA}^{-5}$; 1 au of V_b , or G_b , or $H_b = 627.504 \text{ kcal mol}^{-1}$.